NATIONAL TECHNICAL UNIVERSITY OF ATHENS
SCHOOL OF ELECTRICAL AND COMPUTER ENGINEERING
SCHOOL OF MECHANICAL ENGINEERING

INTERDISCIPLINARY POSTGRADUATE PROGRAMME
"Translational Engineering in Health and Medicine"

The Significance of Carotid Artery Longitudinal Wall Motion: Insights from Block-Matching Ultrasound Analysis

Postgraduate Diploma Thesis
Ioannis Tselios

Supervisor
Dr. Spyretta Golemati
Associate Professor of Biomedical Engineering
National Kapodistrian University of Athens, Medical School

Athens, October 2025

NATIONAL TECHNICAL UNIVERSITY OF ATHENS
SCHOOL OF ELECTRICAL AND COMPUTER ENGINEERING
SCHOOL OF MECHANICAL ENGINEERING

INTERDISCIPLINARY POSTGRADUATE PROGRAMME
"Translational Engineering in Health and Medicine"

The Significance of Carotid Artery Longitudinal Wall Motion: Insights from Block-Matching Ultrasound Analysis

Postgraduate Diploma Thesis
Ioannis Tselios

Supervisor
Dr. Spyretta Golemati
Associate Professor of Biomedical Engineering
National Kapodistrian University of Athens, Medical School

The postgraduate diploma thesis has been approved by the examination committee on *29 October 2025*

1st member	*2nd member*	*3rd member*
Dr. Nikita Konstantina Professor Director of Biomedical Simulations and Imaging Lab, School of Electrical and Computer Engineering, NTUA	Dr. Spyretta Golemati *Associate Professor of Biomedical Engineering* *National Kapodistrian University of Athens, Medical School*	Dr. Manopoulos Christos *Associate Professor* *Director of Biofluid Mechanics Laboratory Fluids Section, School of Mechanical Engineering, NTUA*

Athens, October 2025

Ioannis Tselios

Graduate of the Interdisciplinary Postgraduate Programme,
“Translational Engineering in Health and Medicine”,
Master of Science,
School of Electrical and Computer Engineering,
National Technical University of Athens

Abstract

Cardiovascular disease remains the leading cause of morbidity and mortality worldwide, primarily driven by atherosclerosis. Early identification of vascular dysfunction is therefore clinically important. This thesis investigates carotid artery longitudinal wall motion (CALM) as a functional biomarker of arterial mechanical behavior, using B-mode ultrasound imaging combined with a custom MATLAB speckle-tracking framework. Cine loops from fourteen subjects with carotid atherosclerotic plaques were processed using a multiple kernel block-matching algorithm to extract longitudinal displacement, velocity, and diameter waveforms. Across all subjects, CALM exhibited the characteristic multiphasic pattern of alternating antegrade and retrograde motion. However, amplitudes were consistently reduced compared with reference values for healthy arteries. Peak antegrade displacement measured **0.03 ± 0.01 mm** and peak retrograde **−0.05 ± 0.02 mm**, substantially below the typical physiological range (0.2–1.0 mm). Corresponding peak velocities were also modest (**0.42 ± 0.18 mm/s**) and diameter pulsation was attenuated (**0.29 ± 0.11 mm**), indicating diminished distensibility and localized stiffening in plaque-affected regions. The results demonstrate that CALM quantification is feasible with standard ultrasound imaging and low-complexity computational tools, while capturing functional arterial changes not reflected in structural markers such as intima–media thickness. Overall, this work provides a reproducible processing framework and supports the potential of CALM as a sensitive indicator for early atherosclerotic disease characterization.

.

Keywords: *carotid artery; B-mode ultrasound; longitudinal carotid movement; atherosclerosis;, MATLAB image processing.*

Acknowledgements:

I would like to express my sincere appreciation to Associate Professor, Dr. Spyretta Golemati, my supervisor, for her guidance, constructive feedback, and continuous support throughout the preparation of this thesis. Her expertise and advice were invaluable in shaping this work.

I am also deeply grateful to my family for their encouragement, patience, and unwavering support during my postgraduate studies. Their presence has been essential to the successful completion of this work.

Table of Contents

List of Figures

List of Tables

List of Abbreviations

- CVD – Cardiovascular Disease
- IMT – Intima–Media Thickness
- IMC – Intima–Media Complex
- CALM – Carotid Artery Longitudinal Motion
- ROI – Region of Interest
- BM – Block Matching (motion tracking technique)
- ABM – Adaptive Block Matching
- DBM – Dynamic Block Matching
- OF – Optical Flow (motion tracking method)
- FM – Feature Matching
- NCC – Normalized Cross-Correlation
- fps – Frames per Second
- ECG – Electrocardiogram

1. Introduction

This chapter introduces the reader to the scientific and clinical context in which the present study is situated. It outlines the burden of cardiovascular disease, the role of vascular imaging, and the reasons why carotid artery longitudinal motion is of particular interest. The overall aim of the thesis and its specific objectives are then set out, followed by a brief discussion of its anticipated significance. Finally, the structure of the thesis is presented to guide the reader through the chapters that follow.

1.1 Background and Context

Cardiovascular diseases (CVDs) remain the leading cause of death worldwide, accounting for almost one-third of all global mortality. In Western societies in particular, ischemic heart disease and stroke continue to dominate the health landscape despite advances in therapy and prevention. Although major risk factors such as hypertension, diabetes, smoking, and obesity are well established, the disease process begins silently, often decades before a clinical event occurs.

The central mechanism underlying most CVDs is atherosclerosis. This condition is marked by progressive thickening and stiffening of the arterial wall, and, in advanced stages, by plaque formation and rupture. Importantly, these changes start long before symptoms appear, which makes the search for early, non-invasive indicators of vascular dysfunction an ongoing priority.

The carotid arteries are particularly valuable in this respect. They are superficial and thus easily examined with ultrasound. Moreover, they are among the first vessels where atherosclerotic changes become evident. For this reason, the measurement of carotid intima–media thickness (IMT) has become a routine surrogate for subclinical disease in both research and, in some cases, clinical practice. However, IMT captures only the *static* structure

of the wall. It tells us little about how the wall behaves dynamically under pulsatile blood flow.

In recent decades, attention has shifted to wall mechanics. Most early work focused on radial motion — the familiar systolic expansion and diastolic recoil. By contrast, longitudinal displacement of the arterial wall along its axis was long assumed to be negligible. Yet modern high-resolution ultrasound has challenged this view. Studies have shown that carotid artery longitudinal motion (CALM) is not only detectable but of comparable magnitude to radial motion. Notably, CALM follows a multiphasic pattern during each cardiac cycle and appears sensitive to both aging and disease states.

In parallel, advances in biomedical computing have provided new opportunities for detailed signal and image analysis. Among available platforms, MATLAB stands out for its versatility in handling ultrasound data. With its rich set of libraries for numerical computation and visualization, MATLAB allows researchers to extract displacement waveforms, quantify motion phases, and study reproducibility in a rigorous way. This thesis therefore combines the physiological relevance of CALM with the analytical power of MATLAB.

1.2 Research Aim and Objectives

The overall aim of this study is to investigate the longitudinal motion of the carotid artery wall using ultrasound imaging in combination with MATLAB-based analysis.

To pursue this aim, the study is guided by the following objectives:

- **To review** current research on carotid artery longitudinal motion, with emphasis on its physiological and clinical significance.
- **To describe and classify** the multiphasic displacement waveforms reported in the literature and observed in practice.
- **To evaluate** reproducibility and variability of CALM measurements across time and individuals.

- **To explore** possible mechanisms underlying longitudinal displacement, including the contribution of ventricular–vascular coupling.
- **To develop and apply** MATLAB algorithms for **extracting**, processing, and quantifying CALM from ultrasound recordings.

1.3 Significance of the Study

The significance of this work lies in its focus on a relatively underexplored, yet promising, parameter of vascular function. Several points are worth emphasizing.

First, CALM provides insight into vascular mechanics beyond what is offered by intima–media thickness or radial distension. By examining motion along the vessel axis, the study adds a new dimension to our understanding of how arteries respond to pulsatile blood flow.

Second, CALM has the potential to serve as a clinical biomarker. If proven reliable, it could help identify individuals at increased risk of cardiovascular events before major structural disease develops. This is particularly relevant at a time when preventive cardiology is moving toward earlier and more personalized intervention.

Third, the thesis makes a methodological contribution. By applying MATLAB to ultrasound data, it develops a reproducible computational pipeline that may be adapted in future vascular studies. This intersection of physiology and computation underscores the value of interdisciplinary approaches in advancing cardiovascular diagnostics.

Finally, the study contributes to ongoing discussions about how best to measure vascular health. It does not claim to provide definitive answers but rather to add a carefully constructed piece of evidence to a growing field.

This work complements previous studies by implementing a multi-kernel tracking strategy directly in plaque-affected carotid segments, where motion is

most clinically relevant. Demonstrating that CALM morphology remains preserved while amplitude is significantly reduced provides new insight into how atherosclerosis alters local wall mechanics and supports the potential of CALM as a practical biomarker of arterial stiffening.

1.4 Structure of the Thesis

The remainder of the thesis is organized as follows:

- **Chapter 2: Literature Review** – provides a comprehensive overview of existing work on carotid artery longitudinal motion, its measurement, and proposed mechanisms.
- **Chapter 3: Methodology** – details the dataset, ultrasound imaging procedures, and MATLAB analysis pipeline used in this study.
- **Chapter 4: Results** – presents the findings, including waveform characteristics, reproducibility tests, and subgroup comparisons.
- **Chapter 5: Discussion** – interprets the results, compares them with prior research, and considers implications for physiology and clinical practice.
- **Chapter 6: Conclusion** – summarizes the main contributions of the thesis and outlines avenues for future work.

2. Literature Review

2.1 Cardiovascular Disease and Atherosclerosis

Cardiovascular diseases constitute the major cause of morbidity and mortality in the Western world. Atherosclerosis, a syndrome affecting arterial blood vessels, is characterized by arterial wall stiffening and thickening, is the leading cause for vascular diseases and potentially leads to thrombosis or stroke. In order to increase our knowledge it is important to find methods, preferably noninvasive, to study very early manifestations of vascular disease. Changes in the mechanical properties of arteries can be such a marker of vascular disease. In that aspect, carotid artery is of major importance since it

represents one of the most common sites for the early development of atherosclerosis (Rizi et al., 2020).

The detection and monitoring of pathological changes associated with systemic vascular disorders can be achieved by using a wide range of medical imaging techniques. Among these, ultrasound has become particularly valuable, as it is cost-effective, rapid, non-invasive, free of ionizing radiation, and easily portable. Moreover, its spatial and temporal resolution makes it especially well-suited for examining large arteries such as the carotids.

2.2 Appearance of carotid artery on B-mode ultrasound

Like all elastic arteries, the carotid artery wall is composed of three concentric layers, or tunics, that collectively provide mechanical strength and enable functional adaptation to pulsatile blood flow. These are the tunica intima, tunica media, and tunica adventitia. Each of these contributes to the biomechanical behavior of the vessel in distinct ways. Tunica intima is the innermost layer, consisting of a single layer of endothelial cells lining the lumen of the vessel. Tunica media represents the thickest portion of the carotid artery wall and is composed of concentric layers of smooth muscle cells interspersed with elastic fibers. Tunica adventitia is the outermost layer and comprises primarily connective tissue, including collagen fibers, fibroblasts, and elastic elements (Zahnd et al., 2012a, 2015a, 2017).

On B-mode ultrasound, the wall of the carotid artery is typically visualized as a characteristic double line pattern. The spatial resolution of clinical ultrasound does not allow all three tunics to be separately distinguished. Instead, what is observed are two echogenic (bright) interfaces separated by a relatively hypoechoic (dark) band. The first bright line corresponds to the lumen–intima interface, marking the boundary between flowing blood and the endothelial surface. The intervening hypoechoic band represents the media, while the second bright line corresponds to the media–adventitia interface. Together,

this echogenic–hypoechoic–echogenic sequence is interpreted as the intima–media complex (IMC) (Zahnd et al., 2015a).

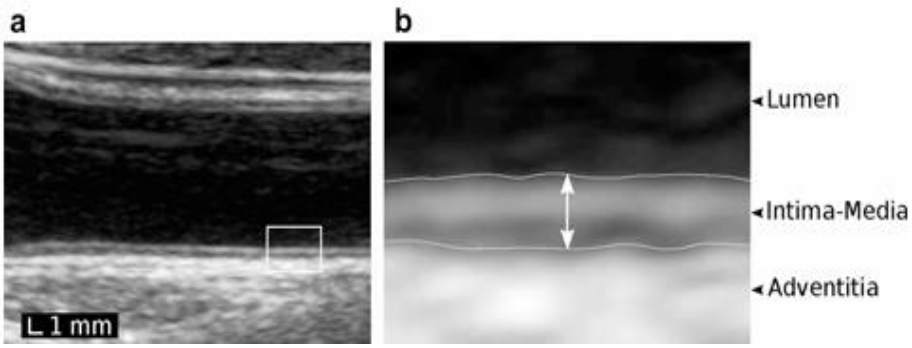

Figure 2. 1: *a*. Longitudinal view of the common carotid artery in B-mode ultrasound imaging, *b*. enlarged region detailing the intima–media complex (Zahnd et al., 2015b).

With modern high-resolution ultrasound, it can be seen that the intima-media complex of the arterial wall moves not only in the radial direction, that is, systolic–diastolic changes in arterial diameter, but also in the longitudinal direction i.e. along the vessel wall.

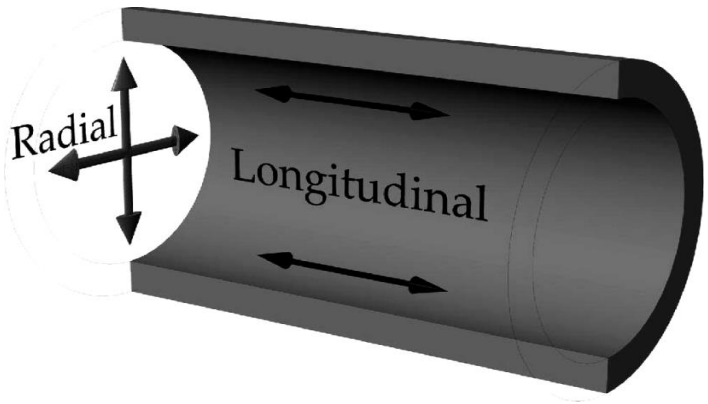

Figure 2. 2: Radial versus longitudinal wall motion (Cinthio et al., 2005).

2.3 Early Research on Longitudinal Motion

In past, longitudinal motion of the carotid artery wall was considered negligible and of little physiological relevance. Early vascular research concentrated almost exclusively on radial motion, since these deformations are relatively large in magnitude, easily detected by conventional ultrasound, and strongly associated with arterial stiffness and blood pressure. Indeed, radial wall movements became an established tool in cardiovascular research, forming the basis for widely applied measures such as pulse wave velocity and arterial distension. These measurements provided reliable estimates of vessel-wall elasticity and were therefore quickly adopted for characterization of vessel wall mechanics (Persson et al., 2003).

By contrast, longitudinal wall displacements attracted little attention, largely because they were assumed to be negligible compared to radial wall movement. Early experimental observations seemed to support this assumption. Initially, cinematography was used to measure longitudinal motion of the abdominal aorta. The movements observed were extremely small. Similar findings were reported in the thoracic aorta. In this case, longitudinal displacements were attributed primarily to respiratory movements of the diaphragm rather than to intrinsic arterial wall mechanics (Persson et al., 2003).

In recent years, with the advent of high-resolution imaging techniques and more sophisticated analysis methods it is possible to detect and quantify subtle axial displacements with sufficient accuracy. In particular, longitudinal movement of the intima – media complex of the common carotid artery is of the same magnitude as the radial movement. These newer observations reveal that longitudinal motion is not only measurable but also follows a complex and repeatable pattern across the cardiac cycle. This has challenged earlier assumptions of irrelevance and suggests that longitudinal wall motion may provide novel and complementary insights into vascular mechanics and cardiovascular risk (Cinthio et al., 2006; Persson et al., 2003).

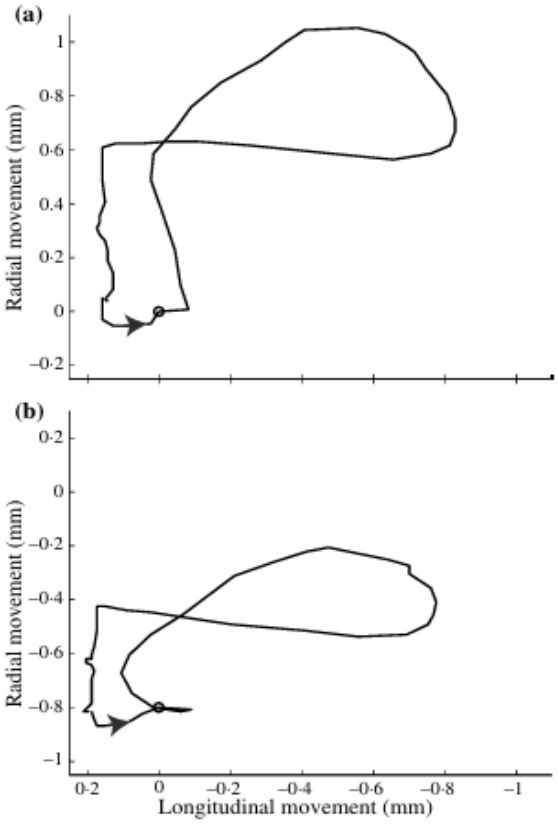

Figure 2. 3:

Longitudinal displacement waveform for the intima-media complex in *a*. the anterior wall and *b*. the posterior wall in the common carotid artery 3 cm proximal to the bifurcation. The rings mark the position of end-diastole. (Persson et al., 2003).

2.4 Longitudinal Motion in Peripheral Arteries

It is worth noting that longitudinal motion is proved to be a generalized phenomenon across vascular tree. Measurements exerted on the abdominal aorta, brachial and popliteal arteries confirm that peripheral vessels exhibit longitudinal movement too. However, the magnitude of longitudinal displacement in peripheral arteries is smaller than the one in the carotid arteries. The reduced amplitudes are attributed to several factors, including structural and physiological differences across the arterial tree, the predominantly muscular nature of the brachial and abdominal arteries, the deeper location of the aorta resulting in a limited frame rate and the smaller displacements relative to the distance from the heart, which make measurements noisier (Cinthio et al., 2005, 2006, 2018a).

2.5 Multiphasic Pattern of CALM

The first thorough characterization of longitudinal motion was performed by Cinthio and his colleagues. Building on earlier methodological work with echo-tracking techniques they studied the common carotid arteries of ten healthy individuals. Vessel wall motion was precisely measured throughout the cardiac cycle, yielding several important findings (Cinthio et al., 2006).

One of the most significant observations was the identification of a multiphasic motion pattern. Longitudinal displacement was shown to follow four distinct phases during each cardiac cycle: an initial anterograde motion in early systole (A1 phase), directed along the flow of blood; a subsequent retrograde displacement later in systole (R phase); a secondary anterograde motion during diastole (A2 phase); and, finally, a gradual return of the vessel wall to its equilibrium position. Importantly, the reproducibility of this multiphasic behavior was validated through ultrasound recordings spanning four to six consecutive cardiac cycles. This characteristic pattern has been also confirmed in later studies (Ahlgren et al., 2012; Au et al., 2018; Cinthio et al., 2018b).

Studying the influence of various risk factors on the magnitude of each directional component of CALM we observe that as the number of cardiovascular risk factors increases the anterograde motion increases and the retrograde motion decreases (Taivainen et al., 2017). Retrograde amplitudes have also been found to correlate inversely with blood pressure, body mass index (BMI), total cholesterol, and triglyceride levels (Taivainen et al., 2018). Furthermore, during the early arterial stiffening process both the systolic anterograde and retrograde components of longitudinal motion are diminished (Yli-Ollila et al., 2016).

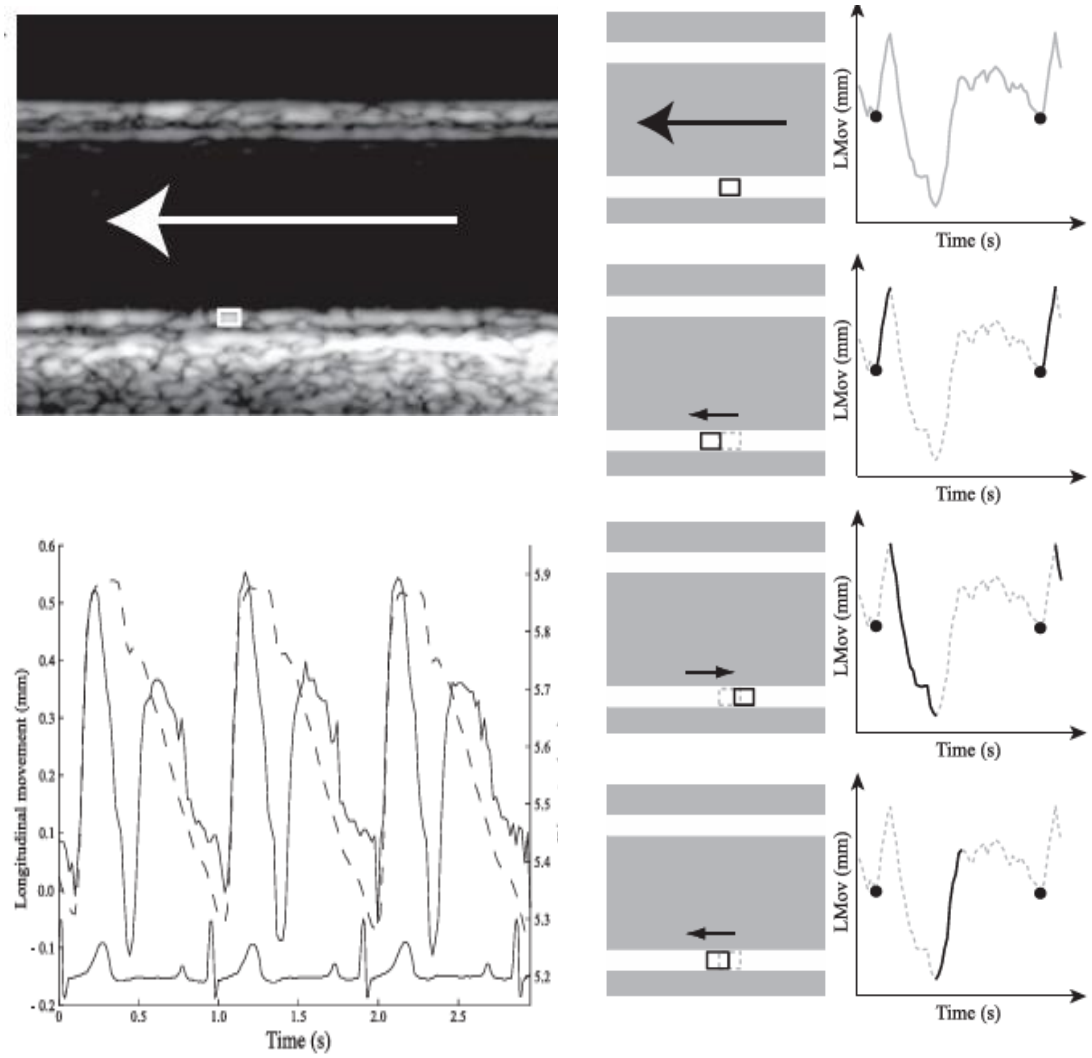

Figure 2. 4: Multiphasic longitudinal displacement pattern (Cinthio et al., 2006).

In addition, two more phases have been denoted in the description of CALM pattern, mainly in patients over 50 years of age. Phase W which is a distinct, rapid retrograde movement starting just before the minimum diameter is seen and is preceding A1 phase. Phase W is more prominent in men 50 – 64 years of age. In men, both the displacement and velocity of phase W increases with age, whereas in women, only velocity is correlated with age Phase X is an anterograde movement or velocity change occurring during, or directly after, the retrograde phase R in the period around, or just before, the dicrotic notch

(when aortic valve closes) is observed in the diameter change curve. This phase is not distinct in all patients, especially not in younger patients, in whom only a barely detectable velocity change or a minimal anterograde movement during retrograde phase R could be observed. In most patients > 50 years of age phase X is a distinct anterograde movement interrupting the retrograde phase R. The displacement and the maximum velocity of phase X increase quadratically with age in both men and women (Cinthio et al., 2018b).

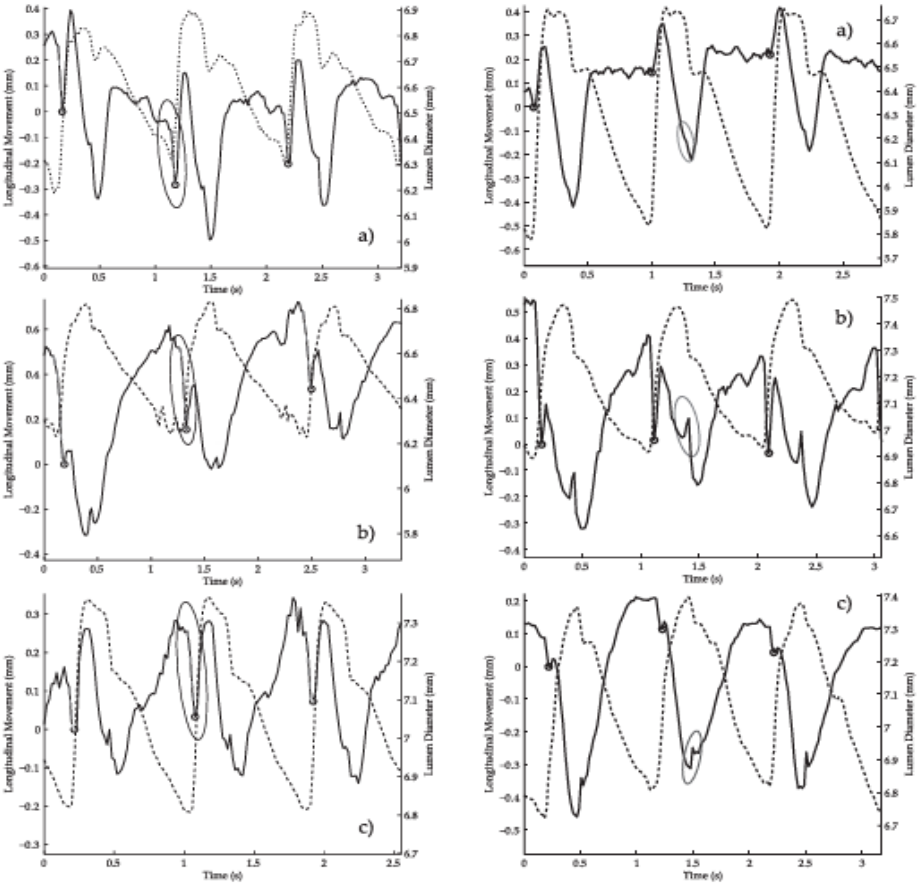

Figure 2. 5: Phases W and X of CALM in older individuals (Cinthio et al., 2018b).

The pattern that describes longitudinal kinetics across the vascular tree differs significantly. In contrast to the carotid artery, longitudinal motion of human abdominal aorta, brachial and popliteal arteries exhibits a biphasic pattern. One possible explanation for pattern difference between CCA and these arteries is the distance to the heart. Both the displacement of the heart in the longitudinal direction and the rotation might have an impact on the aortic arch

and its branches, including the CCA. Since these arteries are located quite a distance from the heart, it is less likely to be influenced by its displacement. The finding that phase X coincides with aortic valve closure also supports the possible effect of the heart (Cinthio et al., 2006).

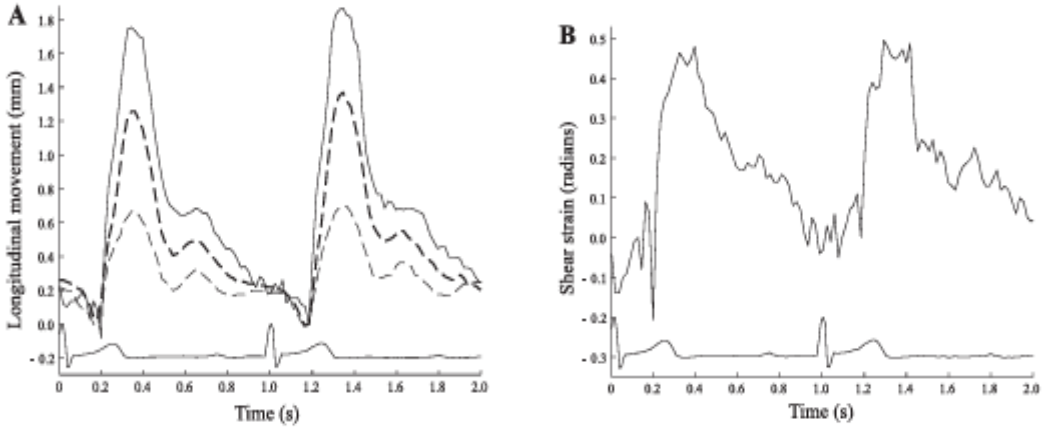

Figure 2. 6: *A.* longitudinal movement of the intima-media (solid line), adventitial region (bold dashed line), and surrounding tissue (dashed line) of the abdominal aorta *B*. cyclic shear strain between the intima-media and adventitial region of the abdominal aorta in the subject in A | ECG bottom trace as reference (Cinthio et al., 2006).

2.6 Patterns of Longitudinal Movement

In individuals under the age of 45 years, there are three distinct motion types that can be identified and are classified as backward-oriented types I and II, and forward-oriented type III. Type I is defined by a very small anterograde displacement in early systole (phase A1), which is markedly smaller than the subsequent retrograde systolic displacement (phase R). An A1/R ratio below 0.3 is used as the criterion for this pattern. In type II, the anterograde phase A1 is relatively larger, though still smaller than the retrograde phase R, yielding an A1/R ratio between 0.3 and 1. By contrast, type III represents a forward-oriented pattern in which the anterograde motion in early systole exceeds the retrograde component, corresponding to an A1/R ratio greater than or equal to 1 (Ahlgren et al., 2012; Cinthio et al., 2006; Yli-Ollila et al., 2013).

In older patients, generally over 55 years of age, two additional displacement patterns have been observed. One such pattern, termed backward-oriented type IV, is characterized by the complete absence of phase A1. Instead of the expected early systolic anterograde displacement, a retrograde motion begins prematurely, even before the end of diastole, well in advance of the usual onset of phase R. This retrograde shift is followed by a diastolic anterograde displacement (phase A2), and in some instances, an additional small phase X can also be discerned. It has been suggested that in this pattern the two retrograde phases, W and R, merge into a single continuous displacement. Type IV shares similarities with type I, and in practice, certain cases are difficult to assign unequivocally to one category, leading to the introduction of a hybrid classification, type I/IV (Ahlgren et al., 2012; Cinthio et al., 2006; Yli-Ollila et al., 2013).

Another novel pattern described in older individuals is the forward-oriented type V. This type is dominated by a large anterograde displacement in early systole (phase A1), with little or no identifiable retrograde phase R. In such cases, phase A1 clearly outweighs the other components, which are often indistinct or absent. Type V has been observed predominantly in older patients, being present more often in individuals over the age of 65. Also it is reported that a pattern of movement similar to type V, seems to be present in patients with atherosclerotic plaques (Ahlgren et al., 2012).

Type	Orientation	A1/R ratio	Defining characteristics	Age group association
I	Backward	< 0.3	Very small anterograde displacement in early systole (A1); dominant retrograde systolic displacement (R).	More common in younger individuals (<45 years).
II	Backward	0.3 – <1	Larger A1 compared to Type I, but still smaller than retrograde R.	Younger individuals (<45 years).
III	Forward	≥ 1	Early systolic anterograde motion (A1) greater than retrograde motion (R).	Younger individuals (<45 years).

IV	Backward	Not applicable	Absence of A1; retrograde motion begins before end-diastole (premature R), followed by diastolic anterograde displacement (A2). Phase X sometimes visible.	More common in older individuals (>55 years).
V	Forward	Not applicable	Dominant large A1 displacement; R absent or indistinct; other phases (A2, X) often unclear.	Predominantly in older individuals (>65 years); rare in younger (<55 years).

Table 1: Patterns of longitudinal movement of carotid artery.

It is obvious that the pattern of longitudinal motion of carotid artery is characterized by large intersubject variability. However, studies have shown that an individual's waveform pattern tends to remain remarkably stable over time. Reproducibility over a four-month period has been demonstrated in adults (Ahlgren et al. 2012), while this observation has been extended to 12 months in children (Au et al., 2019a). Following 12 weeks of supervised exercise training in healthy adults stability of each individual's pattern has also been confirmed (Au et al. 2020). These findings indicate that CALM waveforms may serve as unique "vascular fingerprints" or "vessel signatures," offering complementary information for the assessment of vascular health. It should be noted, however, that a degree of intrasubject variability has been reported, both from beat to beat and across day-to-day measurements.

2.7 Intramural shear strain

Another major contribution of this work was the demonstration of intramural shear stress and shear strain associated with longitudinal motion. Performing measurements at different depths within the arterial wall, including the intima–media complex, adventitia, and adjacent tissues showed that displacement amplitudes decreased progressively with wall depth. This gradient of motion along the layers of arterial wall creates intramural shear forces. Comparisons

between the intima–media and adventitial regions enabled reproducible calculation of the interlayer strain angle, which was approximately one radian. These findings laid the foundation for subsequent investigations into the biomechanical implications of longitudinal shear within arterial tissues (Cinthio et al., 2006).

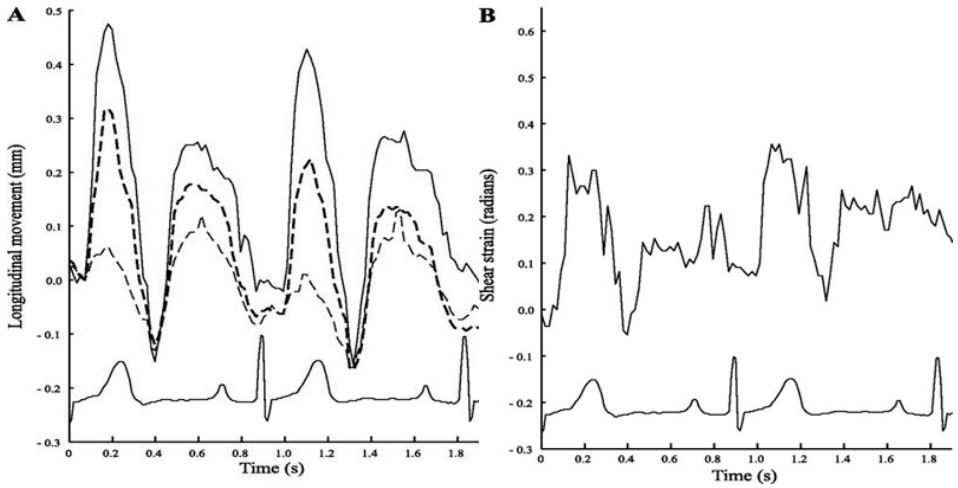

Figure 2. 7: *A.* Depth-dependent longitudinal displacement of the intima-media (solid line), adventitial region (bold dashed line), and surrounding tissue (dashed line) of the common carotid artery, *B.* shear strain between the intima-media and the adventitial region of the common carotid | ECG bottom trace as reference. (Cinthio et al., 2006).

Wall shear strain has been hypothesized to contribute to both the progression of atherosclerosis and the regulation of vasa vasorum circulation. An interesting issue is how the circulation of the vasa vasorum (vessel of the vessels) is influenced by the demonstrated cyclic shear strain/stress within the wall, including the different pattern seen among individuals. The broader influence of longitudinal shear strain and shear stress on vascular health and arterial aging has been further highlighted through theoretical hemodynamic modeling (Athaide et al., 2022; Rizi et al., 2020).

Extending these observations, wall shear strain was compared between elderly diabetic patients, elderly healthy controls and young healthy controls (Zahnd et al., 2011). In both healthy groups, a distinct shearing angle of approximately 1 radian was observed between the intima–media complex and the adventitia, whereas this pattern was markedly attenuated in diabetic

patients, suggesting increased arterial stiffness. Additionally, significantly reduced retrograde shear strain and diminished retrograde displacement of both the intima–media complex and adventitia in individuals with spinal cord injury (individuals with elevated cardiovascular risk) compared with able-bodied controls is reported (Tat et al., 2017). Remarkably, the differences in longitudinal shear strain were independent of group differences in either distensibility or IMT thickness suggesting that intramural shear strain may provide a sensitive marker of early pathophysiological vascular changes that precede the detection of changes in local arterial stiffness or structural thickening.

2.8 Possible Mechanisms of Longitudinal Motion

The multiphasic bidirectional pattern of longitudinal displacement of carotid artery wall suggests that not only opposing forces act simultaneously but also that the size, relation and timing of the individual forces vary throughout cardiac cycle. Forces that have been proposed include shear stress from flowing blood, left ventricular contraction, pulse pressure and smooth muscle cell activation in the arterial wall.Further, the elastic properties and longitudinal tension of the arterial wall are likely to influence all phases of the longitudinal movement. It is also possible that certain phases of the longitudinal movement may be associated with diameter change and elastic recoil. However, interestingly enough longitudinal displacement seems to be independable of wall shear stress (the viscous drag exerted on the vessel wall by the flowing blood) along the carotid artery) (Ahlgren et al., 2012; Au et al., 2016; Cinthio et al., 2006; Fukui et al., 2007).

Another mechanism likely contributing to the longitudinal displacement of the arterial wall was described using a three-dimensional fluid–solid interaction model. Their simulations demonstrated that when the vessel expands radially under pulsatile flow, the arterial wall undergoes local shortening in the longitudinal direction (Fukui et al., 2007). Because the overall vessel length remains constrained, adjacent distal segments are effectively stretched to

compensate, producing a traveling longitudinal wave. This process results in regional retrograde motion, which occurs simultaneously with radial distension. The model further showed that these longitudinal and radial waves interact, and when they coincide, wall shear stress is significantly altered, highlighting the physiological importance of wall dynamics in vascular mechanics.

This concept was later supported experimentally and illustrated an arterial phantom model that as the vessel diameter increases, tissue stretching in the circumferential direction requires recruitment of material from distal regions not yet distended. This recruitment manifests as a retrograde displacement of the wall, consistent with the early systolic retrograde phase of carotid longitudinal motion, sometimes referred to as phase W. Taken together, these findings suggest that longitudinal wall motion may, at least in part, emerge as a secondary consequence of radial expansion (Fukui et al., 2007; Rizi et al., 2020).

Furthermore, the temporal interplay between distinct driving forces appears to underlie the multiphasic waveform of CALM. Current hypotheses propose that left ventricular contraction and relaxation predominantly govern the systolic retrograde (R phase) and diastolic anterograde (A2 phase) displacements, respectively, while the early systolic anterograde displacement (A1 phase) may be attributable to the initial forward blood pressure wave and, to a lesser extent, local smooth muscle activity, despite the sparse presence of smooth muscle cells in the human CCA (Athaide et al., 2022; Au et al., 2016; Cinthio et al., 2018b).

2.9 Ventricular–Vascular Coupling Theory

Although the endocardium (inner lining of the ventricular chamber) is not continuous structurally with the vascular wall of the common carotid artery, the ventricular and vascular systems are anatomically directly linked by the aortic valve at the basal level of the LV, and indirectly by the ejection of blood

from the LV. There seems to be a functional interplay between LV and CCA retrograde movement. There is supportive evidence towards this hypothesis.

The amplitude of longitudinal kinetics in the carotid artery progressively attenuates as we propagate further from the heart to periphery likely due to the distance from LV during systolic contraction. Also, it is reported that taller individuals exhibit less longitudinal motion of the CCA intima-media complex, which is consistent with a reduction in CALM distal to the LV (Gastounioti et al., 2014; Zahnd et al., 2013).

There appear to be temporal associations between CALM events, cardiac mechanics, and carotid hemodynamics. Specifically, the onset of retrograde CALM occurs nearly simultaneously with left ventricular basal septal longitudinal displacement and apical rotation (Au et al., 2016). Furthermore, the transition to anterograde CALM generally coincides with the rise in common carotid artery blood velocity. Peak anterograde displacement usually is observed near peak blood velocity (Au et al., 2016; Au et al., 2017). As the blood velocity wave reaches peak magnitude, peak anterograde CALM displacement occurs, and then retrograde motion resumes.

We can theorize that during this period, the anterograde wall movement represents the interruption of the retrograde cardiac influence by the local mechanical blood velocity force. When the anterograde blood velocity influence is waning, both LV longitudinal and rotational velocities reach peak instantaneous velocity. The now unopposed retrograde forces allow the arterial wall to reach peak retrograde displacement at end-systole. It is worth noting that there are strong statistical associations between the timing of peak retrograde displacement with peak apical and basal rotation of the LV and the timing of peak anterograde displacement with peak blood velocity. (Ahlgren et al., 2012).

It has been proposed that the intersubject variability observed in CALM patterns during systole can be explained by differences in the way cardiac and hemodynamic forces are integrated. In subjects where the cardiac

contribution is dominant, the resulting summated motion profile tends to display a stronger retrograde component, whereas in individuals where the forward blood velocity exerts a greater influence, the overall pattern is characterized by a more pronounced anterograde displacement.(Au et al.2016

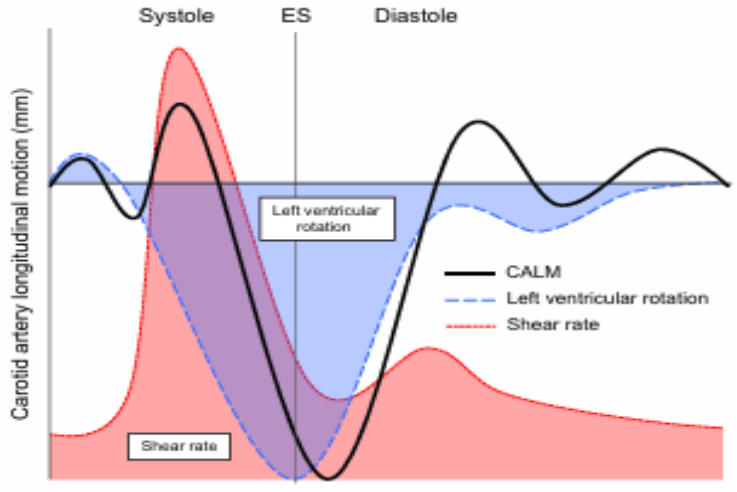

Figure 2. 8: Ventricular–vascular coupling mechanisms underlying CALM (Au et al., 2016).

2.10 Motion Tracking Techniques for CALM

B-mode ultrasound is the most widely recognized imaging modality, producing a gray-scale speckle pattern that conveys structural information, which can be directly visualized on the scanner display. To quantify tissue motion from B-mode image sequences, three tracking strategies are commonly employed: block matching (BM), optical flow (OF), and feature matching (FM).

2.10.1 Block Matching (BM)

Block matching (BM) is one of the most established approaches for motion estimation and has been extensively applied for speckle tracking in ultrasound image sequences. The method relies on identifying, within the (n+1)th frame, the most likely new position of a reference region initially selected in the nth frame. This is achieved by either minimizing a dissimilarity measure, such as

the sum of squared differences, or by maximizing a similarity criterion, such as normalized cross-correlation. Two key parameters play an important role in the performance of BM: the size of the reference region(the kernel) and the extent of the area in which displacement is searched (the ROI) (Golemati et al., 2003).

Early applications of BM to longitudinal wall motion analysis produced relatively coarse displacement waveforms, a limitation attributed to large block sizes and the absence of sub-pixel interpolation. Nonetheless, these studies successfully demonstrated reproducible patterns, thereby confirming the feasibility of in vivo measurements. Later, the “echo-tracking” methods employed smaller block sizes (approximately 0.7×0.7 mm^2), allowing more precise tracking of distinct speckle patterns in high-quality images. However, while reducing block size improves spatial accuracy, it often compromises robustness, particularly in routine clinical settings where image quality is less optimal (Cinthio et al., 2005; Golemati et al., 2003).

Conventional block matching (BM) methods, having a frame-to-frame approach, don’t take into account information from earlier frames. This makes BM particularly vulnerable to speckle decorrelation and tracking errors, especially over longer sequences. To tackle this limitation, adaptive block matching (ABM) techniques were introduced, extending the conventional algorithm by updating the reference block using information from one or more preceding frames. These adaptive methods are typically based on mathematical models that incorporate both a control scheme and an evolution scheme, enabling them to represent expected temporal dynamics while correcting for accumulated errors. Several update strategies have been proposed, including single-frame updating, multi-frame updating, finite impulse response (FIR) filtering, and Kalman filtering. Among these, the Kalman filter has been shown to be the most robust, as it effectively models temporal changes in block location and significantly reduces mean tracking error (Gastounioti et al., 2011, 2013)

Another approach in BM techniques includes the use of multiple blocks. In this strategy, motion is estimated independently from a series of adjacent or partially overlapping kernels at each time step, and the final displacement is computed by averaging these individual estimates. The underlying rationale is to improve robustness by reducing the impact of potential errors arising from any single block. Reported implementations vary in the number of blocks employed, ranging from five and six to as many as sixteen blocks. Obviously, increasing the number of blocks augments robustness but comes at the expense of greater computational cost (Tat et al., 2017; Zahnd et al., 2011, 2012b).

Dynamic Block Matching (DBM) unlike traditional approaches simultaneously estimates motion across the full width of the arterial wall by assigning a block to each image column—often exceeding 350 blocks per frame (Zahnd et al., 2018). Each block undergoes an independent similarity search, generating correlation maps that are subsequently integrated using a dynamic programming framework. This combinatorial analysis extracts the motion of all blocks in order to determine the globally optimal motion field for all points simultaneously, enforcing spatial coherence and reducing local tracking errors. This method enables us to evaluate the motion homogeneity along the vessel length and can provide clinically important information since inhomogeneous longitudinal motion has been associated with cardiovascular risk factors and disease states (Zahnd et al., 2018)

2.10.2 Optical Flow (OF)

Optical flow (OF) estimates the velocity field across successive temporal frames. Whereas block matching (BM) technique tracks a target region dynamically, OF evaluates motion within a fixed spatial window. In the context of carotid longitudinal motion, OF has been successfully applied in several studies (Golemati et al., 2003). While it is reported that the overall waveform shapes derived from OF and BM differed, the timing of their peaks aligned with the same phases of the electrocardiogram (ECG). Moreover, BM generally yielded greater estimates of maximum velocity and displacement in

both radial and longitudinal directions, with the discrepancy between OF and BM being particularly pronounced in the longitudinal direction (Rizi et al., 2020).

2.10.3 Feature Matching (FM)

A novel method for motion tracking based on the automatic extraction of salient image regions was recently proposed. This approach employs detectors such as scale-invariant feature transform (SIFT), speeded-up robust features (SURF), and maximally stable extremal regions (MSER) to identify target points. Its main strength lies in robustness, as tracking is restricted to salient points that are re-selected at every time step, thereby reducing the influence of poorly defined features. Furthermore, feature matching (FM) enables shear strain assessment across different anatomic layers by tracking points within distinct wall regions, providing depth-specific shear evaluation similar to that achievable with certain block-matching methods. However, FM needs continuous re-selection of feature points, which hinders precise single-point tracking and prevents the generation of a dense displacement field (Rizi et al., 2020).

2.11 Clinical Studies on CALM

Accumulating evidence indicates that longitudinal motion provides additional value for cardiovascular risk assessment. There are multiple associations between carotid wall longitudinal motion and vascular health. One of the most widely used indices is the peak-to-peak motion amplitude which is consistently linked to cardiovascular status, while remaining independent of established risk factors, conventional non-invasive measures of arterial stiffness, and markers of subclinical carotid atherosclerosis (Svedlund & Gan, 2011; Taivainen et al., 2017; Zahnd et al., 2012b).

More specifically, the amplitude of longitudinal motion has been shown to vary with age, following an inverted U-shaped relationship (Au et al., 2019b; Zahnd et al., 2018). Significantly reduced amplitudes have been reported in elderly

patients with coronary artery disease (0.54 mm vs. 0.11 mm) (Svedlund & Gan, 2011), in elderly diabetic patients (0.48 mm vs. 0.31 mm) (Zahnd et al., 2011), and in adults with periodontal disease (0.42 mm vs. 0.15 mm) (Zahnd et al., 2012b). Further, reductions in peak-to-peak amplitude have been observed in association with coronary artery disease and myocardial ischemia, independent of arterial stiffness (Au et al., 2017). Pharmacological interventions seem to influence longitudinal wall motion, as catecholamine administration and beta-blockade induced marked changes in displacement amplitude and intramural shear strain in porcine carotid arteries (Ahlgren et al., 2009, 2012). More specifically, increase in longitudinal displacement seems to be strongly related to a-adrenoreceptor activation (Ahlgren et al. 2009).

There are studies reporting an inverse relationship between systolic blood pressure and both the peak-to-peak and retrograde amplitudes (Taivainen et al., 2018; Yli-Ollila et al., 2013). Moreover, peak-to-peak and retrograde amplitudes were positively associated with carotid artery distensibility and inversely associated with pulse wave velocity, independently of brachial flow-mediated dilation and intima–media thickness (Taivainen et al., 2017). Notably, peak-to-peak amplitude was also found to predict one-year cardiovascular outcomes in patients with suspected coronary artery disease, independently of cross-sectional stiffness and intima–media thickness (Svedlund & Gan, 2011).

In pediatric populations, longitudinal motion was only weakly correlated with arterial stiffness, suggesting it is not a reliable surrogate marker of stiffness in children (Proudfoot et al., 2019). Similarly, evidence from multi-ethnic cohorts suggested that longitudinal displacement may predict coronary heart disease and cardiovascular events, although associations did not consistently reach statistical significance (Gepner et al., 2015, 2019). Finally, spatial heterogeneity has been observed along the arterial length: peak-to-peak amplitude was consistently lower in wall regions located further from the heart

compared with more proximal sites, possibly reflecting a progressive attenuation of the driving forces along the artery (Zahnd et al., 2015b).

Associations between longitudinal motion and arterial distension have also been studied. Diameter change in the common carotid artery has a partly linear relationship to the longitudinal motion of the intima-media complex and is thus a potential initiating force for the longitudinal motion. Stable phase difference has been noticed between the blood pressure signal and longitudinal motion, hence suggesting a direct association between longitudinal motion and arterial stiffness (Yli-Ollila et al., 2016).

3. Methodology

This chapter outlines the methodological framework implemented to quantify the longitudinal motion of the carotid artery wall using B-mode ultrasound cine loops. The goal was to extract reliable displacement and velocity waveforms from ultrasound videos through robust image processing, motion tracking, and signal analysis.

3.1 Data Acquisition

Fourteen longitudinal-view B-mode ultrasound cine loops/ frames of the carotid arteries were analyzed. Each video was exported in AVI/ TIF format, containing multiple cardiac cycles. The frame rate was read from video metadata using MATLAB's VideoReader.FrameRate. In some cases, metadata were missing or implausible. Since an incorrect frame rate would compromise velocity estimation and synchronization with the cardiac cycle, a manual override of 35 frames per second (fps) was implemented. This choice reflected the nominal cine acquisition frame rate of the ultrasound system and corresponded to its displayed sweep speed. It also lies within the standard range of clinical B-mode recordings of superficial arteries (30–40 fps),

ensuring adequate temporal resolution (≈28.6 ms per frame) to resolve both systolic acceleration and diastolic recoil without aliasing.

3.2 Spatial Calibration

Spatial calibration was derived from the displayed imaging depth. The total depth in millimeters was divided by the image height in pixels to obtain the axial resolution (mm/pixel). Since exported AVI/ TIF files use square pixels, it was assumed that lateral and axial pixel spacing are equal. Under this assumption, the same calibration factor was applied to both axes, allowing pixel displacements along the longitudinal axis to be expressed in physical units (mm).

3.3 Region of Interest Selection

Each cine loop/ frame was imported into MATLAB (MathWorks, Natick, MA, R20xx) and converted to grayscale. The first frame of each sequence was displayed, and the operator manually defined a thin (approximately 1,2 mm) horizontal region of interest (ROI) across the far wall of the artery. ROI placement was carefully performed to avoid atherosclerotic plaques where possible. This ensured that the region corresponded to the intima–media complex and minimized background interference.

3.4 Kernel Tiling

The ROI was subdivided into rectangular kernels of 40 × 10 pixels, tiled horizontally with a stride of 12 pixels. This configuration resulted in ~70% overlap between adjacent kernels, improving redundancy and robustness against speckle decorrelation. Kernels were centered vertically at the midpoint of the ROI to ensure alignment with the arterial wall. The ROI defines the anatomical extent of the analysis along the arterial wall, whereas kernels

represent the smaller windows of pixel intensities used by the block-matching algorithm to estimate local speckle motion between frames.

3.5 Motion Tracking by Normalized Cross-Correlation

For each frame pair, longitudinal motion was estimated using normalized cross-correlation (NCC) block matching. For a kernel T extracted from frame It, candidate patches of the same size were searched in frame It+1 within a ±10-pixel horizontal window. This search range covered the physiologically expected inter-frame motion (<1mm) while limiting spurious matches.

The NCC coefficient was defined as:

$$NCC(A,B) = \frac{\Sigma(A-\bar{A})(B-\bar{B})}{\sqrt{\Sigma(A-\bar{A})^2 \cdot \Sigma(B-\bar{B})^2)}}$$

where *A* denotes the pixel-intensity values within the kernel in the current frame and *B* denotes the pixel-intensity values within the corresponding search region in the subsequent frameThe displacement corresponding to the maximum correlation was taken as the best estimate. Sub-pixel accuracy was achieved by fitting a quadratic curve to the correlation peak and its two neighbors.

After estimation, each kernel was repositioned horizontally by its displacement to maintain tracking of the same speckle pattern across frames. Vertical positions were fixed to ensure consistent wall alignment.

3.6 Outlier Rejection

Tracking reliability was enforced in two stages. First, kernels with peak NCC below 0.65 were discarded. Second, outliers were rejected using the median absolute deviation (MAD) criterion. A kernel was retained if:

$$| s_i - \bar{s} | \leq 2.5 \times 1.4826 \times MAD$$

where $\bar{s}$ is the median of the set. The retained displacements were summarized by their median, yielding the net longitudinal shift per frame.

3.7 Displacement and Velocity Signals

Cumulative displacement was obtained by summing frame-to-frame shifts and converting pixels to millimeters using the calibration factor. To remove baseline wander due to probe drift, a moving median filter with a 1.5-second window was subtracted. The drift-free displacement was then smoothed using a Savitzky–Golay filter which preserves waveform morphology while attenuating noise.

Velocity (v(t)) was computed as the temporal derivative of displacement (x(t)):

$$v(t) = -\frac{d}{dt}x(t)$$

and smoothed using the same filter.

3.8 Outputs and Quality Control

For each sequence, three outputs were generated:

1. **Displacement and velocity time series** (mm, mm/s).
2. **Kernel acceptance rate** (% of valid kernels per frame).
3. **Annotated images** of the ROI and kernels.

All results were exported as CSV tables (frame index, time stamp, displacement, velocity, acceptance) and PNG diagnostic plots, ensuring reproducibility and transparency.

3.9 Assumptions and Limitations

In order to ensure robust and reproducible analysis, the proposed methodology is based on several assumptions. Certain limitations have to be taken into account also:

- Exported AVI/ TIF pixels are assumed to be square, so axial and lateral calibration are equal.
- ROI placement is user-dependent, thus affecting reproducibility of the results.
- Manual override of 35 fps is valid when metadata are missing or implausible.

These assumptions may introduce small errors, particularly under probe drift or heterogeneous plaque morphology, but were necessary to ensure robust and reproducible analysis.

4. Results

4.1 Overview of Findings

Across all examined carotid artery segments, speckle-tracking performance was consistently strong, with kernel acceptance remaining close to or at 100% in nearly every case. This ensured reliable capture of subtle arterial wall motion even in the presence of atheromatous plaque. Both radial (diameter) and longitudinal motion waveforms showed clear synchronization with the cardiac cycle, confirming physiologically valid measurements throughout the dataset.

While cyclic distension was always observable, its magnitude was uniformly modest, indicating reduced arterial compliance in plaque-affected regions. Longitudinal motion demonstrated the expected alternating antegrade and

retrograde phases characteristic of CALM behaviour, yet with attenuated excursion. Arterial wall mechanics were therefore preserved in timing and phase structure but diminished in amplitude. Overall, the findings highlight a consistent biomechanical pattern across subjects: the vessel remains responsive to pulsatile loading but is mechanically constrained due to localized stiffening associated with atherosclerotic disease.

4.2 Summary of CALM Characteristics

All subjects exhibited the characteristic multiphasic pattern of carotid arterial longitudinal motion. The displacement traces generally opened with a systolic retrograde pull, followed by a transition to antegrade movement and secondary oscillations during diastole. This conserved shape across participants demonstrates that plaque-affected segments continue to engage in shear-driven wall sliding despite structural changes.

However, the scale of this motion was markedly reduced in every case. Peak displacement typically remained well below ranges expected for healthy carotids. The damping of motion was most pronounced at and immediately downstream of plaque, where stiffness and altered force propagation restrict the ability of the intima–media to glide along the adventitial structures. In contrast, distal regions sometimes showed gradual motion recovery, supporting the interpretation that plaque influence is spatially dependent. Overall, CALM morphology remained intact, but its mechanical expression was muted throughout the cohort, reflecting the widespread effect of atherosclerosis on wall deformation.

The following table summarises CALM characteristics for the full cohort into a single representative description of mechanical behaviour.

Subject	Kernel Acceptance	Diameter Behaviour	Longitudinal Motion Behaviour	ROI Location (most representative)	Overall Interpretation
1	100%	Minimal but clear systolic expansion	Coordinated multiphasic motion with low excursion	Downstream of plaque	Preserved timing; motion amplitude suppressed by stiffness
2	100% (L/R)	Slight asymmetry; R > L	Multiphasic motion on both sides; slightly greater amplitude on right	Downstream of plaque shoulder	Asymmetric stiffening; right wall retains more mobility
3	100%	Subtle pulsatility	Low-amplitude but structured waveform	Downstream of plaque	Transitional attenuation of axial sliding
4	>95%	Abrupt early deformation then damping	Strong initial axial shift followed by truncated recovery	Near plaque	Local mechanical restriction from stiff plaque
5	>95%	Moderate pulsatile response	Stable multiphasic oscillations with reduced displacement	Distal to plaque	Partial mechanical recovery further from lesion
6	70–100% (L), 100% (R)	Very limited on left; slightly improved on right	Low-amplitude controlled oscillations; right side better preserved	Near plaque shoulder	Irregular stiffening; side-dependent mechanical impact
7	100%	Minimal radial shifts	Small, consistent multiphasic patterns	Downstream of plaque	Downstream stiffening significantly dampens motion
8	100% (L/R)	Slightly higher wall response on left	Phasic motion intact; right side more constrained	Adjacent to eccentric plaque	Regional asymmetric stiffness with preserved phasing

9	100% (L/R)	Very faint pulsations bilaterally	Markedly reduced but coherent motion	Downstream of plaque	Highly restricted wall mobility; persistent coordination
10	100% (L/R)	Slow and shallow deformation	Truncated oscillatory behaviour throughout the cycle	Adjacent to plaque	Chronic suppression of axial wall sliding
11	>95–100% (L/R)	Small monotonic diameter variation	Limited but synchronised motion patterns	Plaque proximity	Bilateral uniform stiffening influence
12	100%	Flattened diameter waveform	Minimal longitudinal motion excursions	Adjacent plaque region	Severe mechanical limitation with residual coordination
13	100%	Reduced and uneven expansion	Accurate timing but diminished axial range	Near plaque	Advanced stiffening; motion preserved but very restricted
14	100%	Negligible pulsation	Lowest amplitude observed; timing preserved	Adjacent to plaque	Near-fixed wall behaviour with intact cardiac response

Table 2: Summary of CALM displacement and velocity characteristics per subject.

ROI Location refers to the position of the motion-tracking region relative to plaque geometry and hemodynamic flow direction. “Near plaque” indicates the most mechanically restricted zone, while “distal” and “downstream” regions allow evaluation of motion propagation beyond the stiffened segment.

These descriptors are important because wall-motion behaviour changes depending on where the vessel is mechanically constrained. The categories used in this table are defined as follows:

Term Used	Meaning	Biomechanical relevance
Near plaque	ROI positioned directly over or immediately adjacent to the plaque mass	Represents zones of highest stiffness and most restricted wall motion
Downstream of plaque	ROI located just distal to plaque in the direction of blood flow	Captures how altered hemodynamics and tethering effects propagate beyond the lesion
Downstream of plaque shoulder	Tracked just below the sloping edge of plaque where shear stress changes rapidly	Shoulder regions often show transitional mechanics and abrupt changes in motion amplitude
Adjacent to eccentric plaque	ROI placed near a non-uniform or asymmetrically distributed plaque	Asymmetric loading leads to side-dependent differences in wall compliance
Distal to plaque	ROI sufficiently downstream where plaque influence is reduced	Used to observe potential recovery in longitudinal wall mobility
Near plaque shoulder	Tracking positioned at the boundary between plaque and healthy tissue	Common site for motion suppression due to stiffness gradients
Plaque proximity	A general descriptor when exact geometric boundaries are difficult to delineate	Indicates motion is still within plaque-affected mechanics

Table 3: Explanation of ROI location differences.

4.3 Subject-Specific Results

4.3.1 Subject 1

In Subject 1, the carotid diameter waveform shows a relatively small change during each cardiac cycle, around 0.1–0.2 mm. The signal is not very smooth, and the distension velocity includes sharp fluctuations, which suggests that the artery does not expand and recoil in a uniform way. This behavior fits with the presence of plaque and a more rigid arterial segment.

The longitudinal motion pattern also shows limited movement, roughly ±0.05 mm, with less distinct systolic and diastolic phases than expected. The wall seems to slide only slightly along its axis, which points to reduced flexibility and restricted motion of the affected segment. Tracking quality appears stable based on the high kernel acceptance rate, meaning the motion estimation is reliable for this subject.

In summary, this carotid artery shows a combination of reduced diameter change and limited longitudinal motion, indicating stiffening and altered wall behavior consistent with plaque influence.

Figure 4. 1: Subject 1 – ROI placement

4.3.2 Subject 2

For this subject, both the left and right carotid arteries show relatively small diameter changes, generally around 0.03–0.05 mm. The waveform includes noticeable irregular dips and peaks, suggesting that the artery does not expand smoothly with each heartbeat. The distension velocity varies rapidly as well, which points to uneven wall deformation influenced by the plaque.

Longitudinal movement is also limited on both sides. The displacement curves show modest axial sliding, typically around ±0.05–0.08 mm, and the motion pattern lacks a clear, repeatable rhythm. This reduced and inconsistent movement indicates that the arterial wall may be more constrained and less flexible. Tracking performance was mostly stable, with a high kernel acceptance rate, so the motion measurements appear reliable.

Overall, both carotid arteries in Subject 2 show restricted motion and irregular expansion, reflecting the mechanical impact of plaque on the vessel walls.

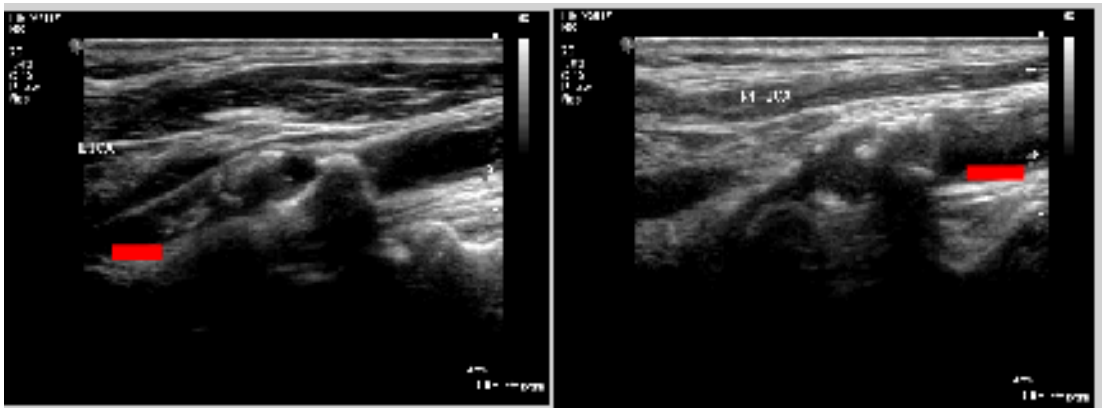

Figure 4. 2: Subject 2 – Left and Right ROI placement..

:

4.3.3 Subject 3

The diameter waveform in Subject 3 shows a very small change during each heartbeat, mostly within ±0.05 mm. The signal stays flat for long periods, and then suddenly dips more noticeably toward the end of the recording. The distension velocity also becomes noisier there, suggesting that the wall is

reacting less uniformly, likely due to stiffness from plaque. The longitudinal motion is quite limited. The wall slides only a few tenths of a millimeter back and forth, and there is no strong repeating pattern tied to the cardiac cycle. This points to a restricted mobility of the vessel wall. Tracking remained highly stable throughout, so the data looks trustworthy.

Overall, Subject 3 shows reduced radial expansion and minimal longitudinal motion, reflecting a stiffened arterial segment with altered mechanical behavior.

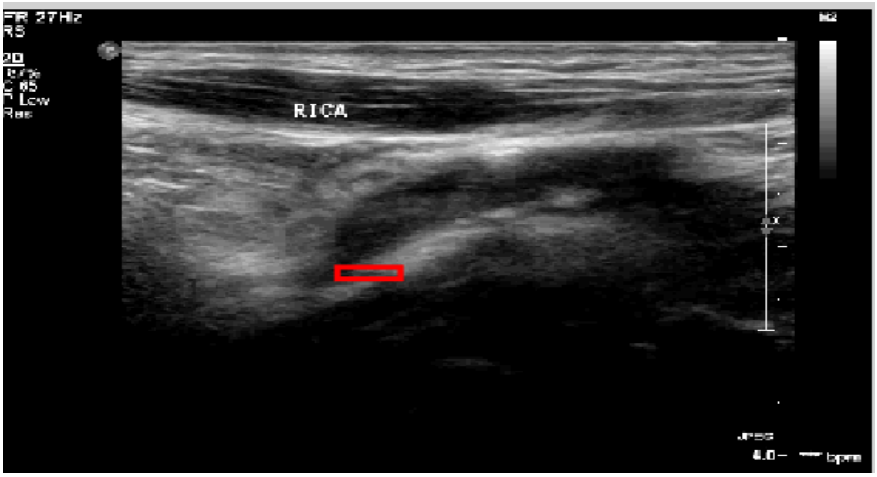

Figure 4. 3: Subject 3 – ROI placement.

4.3.4 Subject 4

In Subject 4, the diameter varies slightly more than in Subject 3, but it is still on the lower side — roughly within ±0.05 mm. The waveform is moderately irregular, especially around peaks and troughs, indicating uneven expansion along the wall. The longitudinal motion is also restricted, around ±0.07–0.1 mm. The signal has some rhythm matching the cardiac cycle, but the wall still appears somewhat constrained. Velocity changes become sharper at certain phases, suggesting variable wall loading depending on where the plaque stiffens the structure. Kernel acceptance was steady, confirming robust tracking.

In summary, Subject 4 shows clear signs of reduced flexibility in both radial and longitudinal behavior, although slightly more motion is preserved compared with Subject 3.

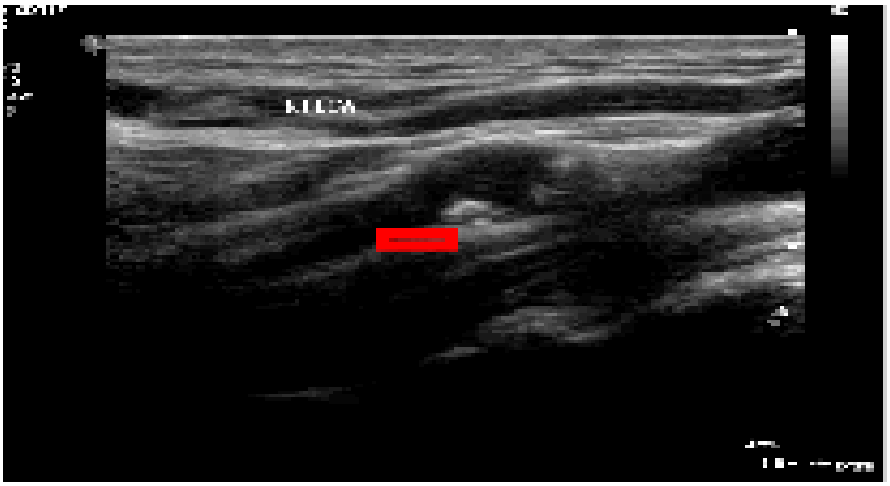

Figure 4.4: Subject 4 - ROI placement.

4.3.5 Subject 5

The diameter waveform in Subject 5 shows relatively small changes during each heartbeat, typically within ±0.15–0.2 mm. There are noticeable drops around the mid-recording, where the vessel seems to compress more abruptly, suggesting the wall is not responding in a smooth, elastic way. The distension velocity becomes noisy when these dips occur, which fits with a more rigid or uneven wall segment. Longitudinal motion shows a modest sliding amplitude, roughly within ±0.08 mm. The pattern does follow the cardiac rhythm, but the movement is still fairly restricted, indicating the wall does not glide freely along its length. Velocity shifts are sharper around peaks, hinting at changing mechanical load in that region.

Tracking performance appears very stable over time, so the measured motion is considered reliable. Overall, Subject 5 presents reduced radial expansion and limited axial movement, both pointing toward a stiffer arterial wall influenced by plaque.

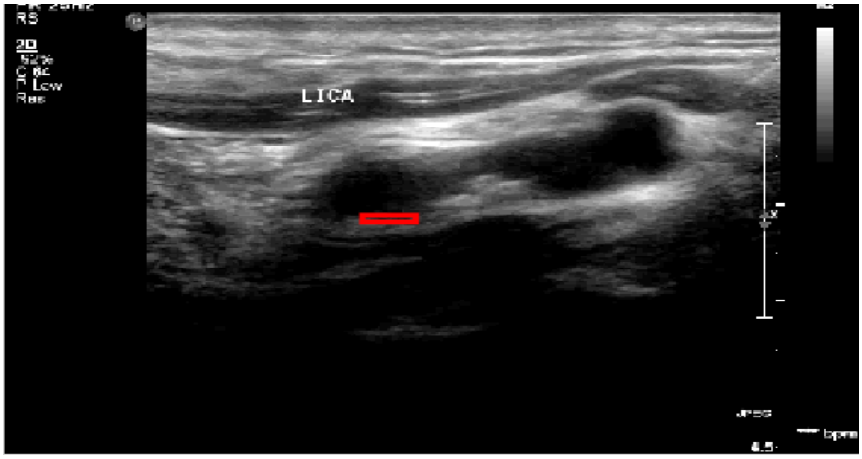

Figure 4. 5: Subject 5 – ROI placement.

4.3.6 Subject 6

For this subject, the left carotid shows a sharp early drop in diameter followed by a long interval with very little deformation. The diameter change stays mostly flattened after the first second, and the velocity signal becomes low and irregular, indicating the wall is not expanding normally. Longitudinal motion is also quite small, generally only a few tenths of a millimeter, which suggests reduced wall mobility.

The right carotid presents slightly more dynamic behavior. The diameter waveform shows more frequent pulsatile changes and larger peaks compared with the left side, though still limited overall. The longitudinal motion follows the cardiac cycle more clearly here but is still restricted, meaning the arterial wall remains mechanically constrained. Tracking quality was good on both sides — occasional drops in kernel acceptance occurred, but the majority of frames were reliable.

Overall, Subject 6 displays limited arterial deformation on both sides, with the left carotid appearing more stiff and less responsive than the right. The wall motion in both arteries reflects the mechanical impact of atherosclerotic plaque.

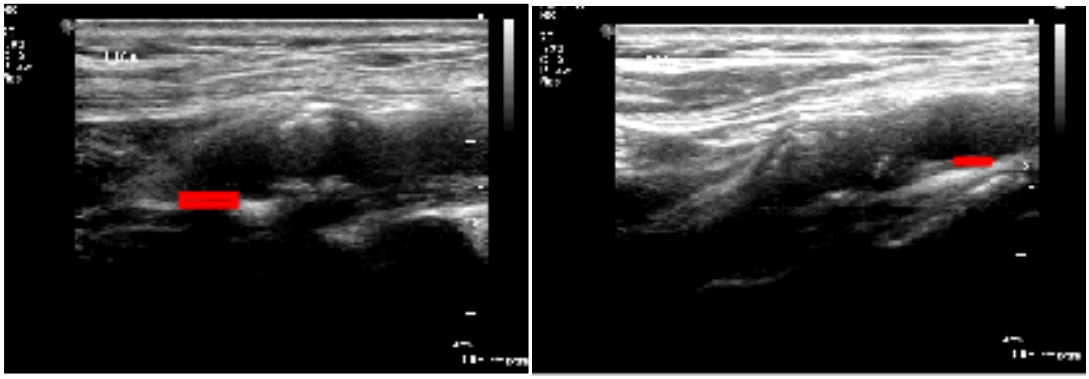

Figure 4. 6: Subject 6 – Left and Right ROI placement.

4.3.7 Subject 7

For Subject 7, the carotid diameter changes remain quite small and inconsistent throughout the recording. The waveform includes brief dips and peaks, but there is no strong, repetitive pulsatile behavior, which suggests limited arterial compliance in the tracked segment. The distension velocity signal also shows rapid fluctuations, pointing to uneven wall mechanics.

The longitudinal motion signal presents clear cardiac cycling, but the overall amplitude remains modest. The wall moves back and forth with a limited range, giving the impression that the segment is not able to slide freely due to stiffening. Kernel tracking stability was good, confirming that the extracted motion reflects real vessel behavior.

Overall, Subject 7 demonstrates mild pulsatility with restricted longitudinal motion, consistent with a stiff and plaque-affected artery.

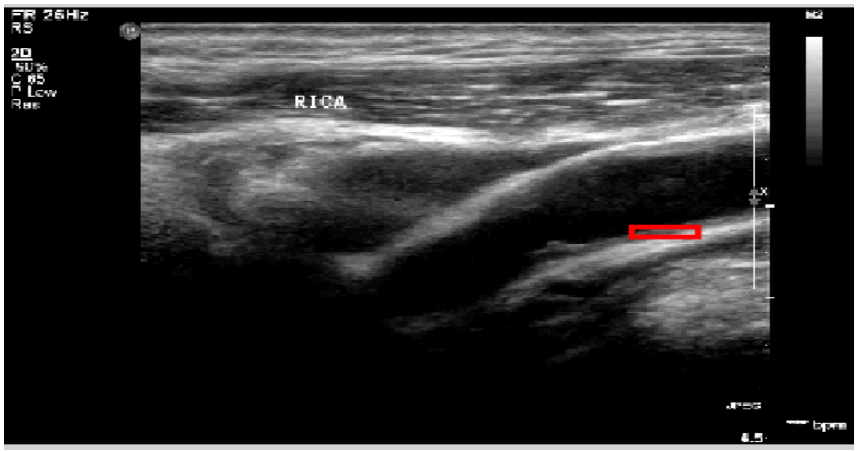

Figure 4. 7: Subject 7 – ROI placement.

4.3.8 Subject 8

The left carotid artery shows noticeably reduced diameter variation, with most of the waveform remaining near baseline and only small expansions during systole. The dips are sharper than the rises, suggesting the artery may collapse more easily than it expands — a sign of compromised elasticity. Distension velocity spikes occasionally but remains low and scattered otherwise.

Longitudinal displacement is also quite limited, staying mostly within a small amplitude. Although the cardiac pattern is visible, the movement appears dampened and somewhat asymmetric between cycles. Kernel acceptance held stable through the sequence, so the tracking can be considered reliable.

Furthermore, the right carotid shows very limited diameter change for most of the recording. Only near the last second does the vessel show a sharper drop and a larger recovery, suggesting a delayed and uneven response to the pulse. The distension velocity spikes around those drops indicate abrupt mechanical loading, likely where the plaque is more restrictive.

Longitudinal motion is present but small in amplitude, with a somewhat weakened cardiac rhythm. The motion looks dampened and progressively

flatter toward the end of the clip, implying reduced wall freedom to slide. Kernel acceptance stays high until brief losses near the end, so overall tracking remains reliable.

In conclusion, both sides show reduced deformation, with the right artery behaving slightly more unevenly — a sign of localized stiffening from plaque.

Figure 4. 8: Subject 8 –Left and Right ROI placement.

4.3.9 Subject 9

In left carotid, the diameter waveform is very flat, indicating minimal radial expansion through most of the cardiac cycles. Only toward the last second does the waveform show a moderate rise, while the distension velocity remains low and scattered, both pointing to a stiff vessel segment.

The longitudinal displacement shows a bit more motion than the diameter does, but still remains limited. The cycles are not strongly defined, and the vessel appears to return slowly rather than snapping back — another hint of reduced elasticity. Tracking was stable, confirming that the measurements reliably reflect the arterial behavior.

The left carotid behaves as a mechanically restricted artery with low compliance and limited wall motion, consistent with plaque influence.

The right carotid shows slight but noticeable diameter variation, though still lower than what would be expected in a healthy artery. There are a few sharper downward movements in the waveform, which indicates uneven wall

behavior under pulsatile pressure. Distension velocity also becomes more erratic during those drops, reflecting localized stiffness. Longitudinal motion shows a clear cardiac rhythm but remains limited in amplitude. The displacement curve flattens between cycles, suggesting the arterial wall does not fully recover or glide freely.

Kernel tracking was stable throughout, validating the measurements. Overall, the right carotid exhibits modest axial motion and reduced radial distension, consistent with a stiff, plaque-affected segment similar to the left side — although slightly more motion is preserved here.

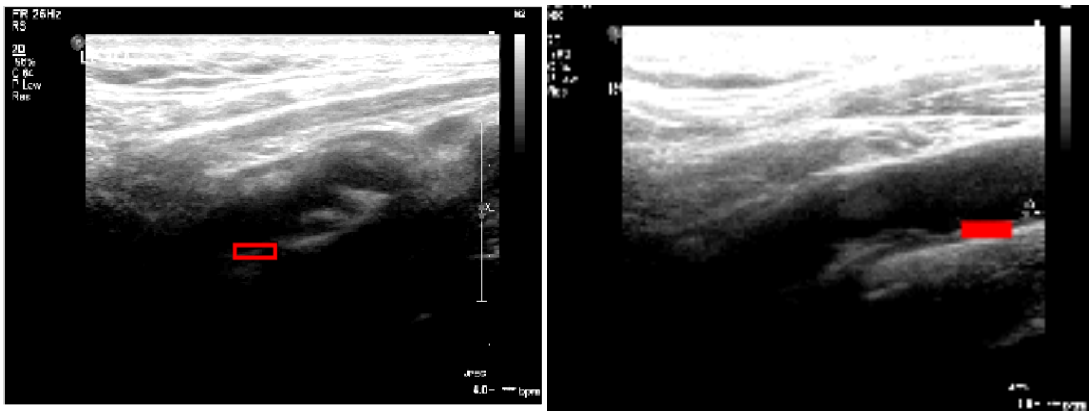

Figure 4. 9: Subject 9 – Left and Right ROI placement.

4.3.10 Subject 10

The carotid diameter signal shows minimal expansion, staying close to baseline for most of the recording. The vessel only shows small rises near mid-cycle, and the waveform is mostly flat, which indicates reduced compliance. The distension velocity confirms this with low, irregular variations and occasional sharper spikes.

Longitudinal displacement has a slightly better-defined pattern than the diameter change, but amplitude remains low overall. The wall moves in a restricted sliding manner, without the smooth, wide excursions expected in a more elastic segment.

Kernel acceptance remained high, indicating confident tracking. In summary, Subject 10 demonstrates clinically small arterial motion in both radial and longitudinal directions, suggesting a mechanically stiff artery due to plaque presence.

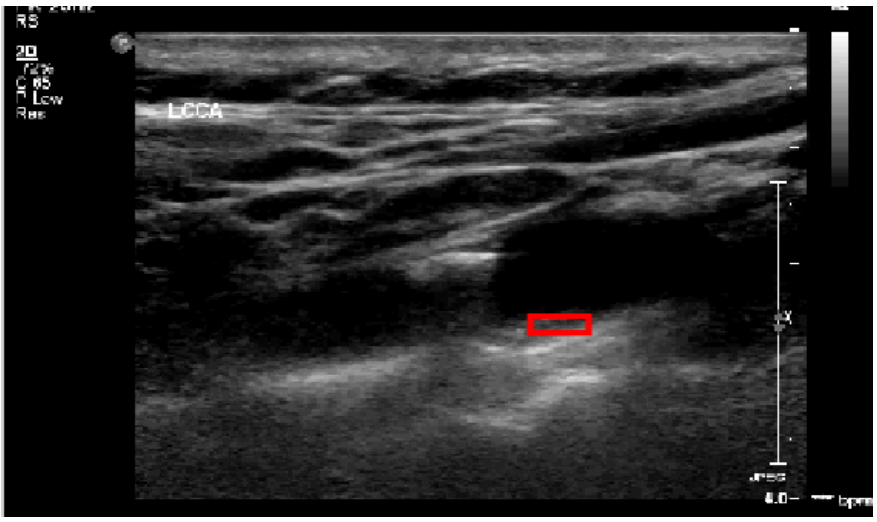

Figure 4. 10: Subject 10- ROI placement.

4.3.11 Subject 11

For the left internal carotid artery, tracking stability was consistently high with kernel acceptance maintained above 95%, supporting confidence in the speckle-tracking output. The diameter waveform displayed a subtle but clearly identifiable cyclic expansion–contraction behavior, though the absolute change remained small (around ±0.05 mm), suggesting limited radial compliance. Longitudinal displacement showed a regular multiphasic structure with alternating motion toward and away from the heart. Peak antegrade excursion reached approximately +0.05 mm, whereas the retrograde component extended to about −0.10 mm. The corresponding velocity profile followed the same rhythm, with modest peaks around ±0.3 mm/s. Although the amplitude was subdued, the motion pattern remained physiological in shape, implying that the ROI was positioned in a region influenced by plaque stiffness but still capable of sustaining coordinated wall motion.

On the right side, kernel acceptance again remained fully stable. The diameter trace exhibited slightly more pronounced variation than on the left side, indicating a small degree of preserved radial distension. Longitudinal wall displacement followed a characteristic antegrade motion during systole, reaching about +0.04 mm, followed by a clear retrograde recovery around −0.06 mm. The velocity waveform echoed this dynamic, with smooth transitions and peak velocities up to ±0.4 mm/s. The presence of plaque appeared to dampen the amplitude of both phases while preserving fundamental motion timing. Notably, the waveform remained highly consistent across cycles, suggesting a robust mechanical coupling to the cardiac cycle despite structural wall changes. Overall, both sides of Subject 11 demonstrated reduced but well-coordinated CALM dynamics.

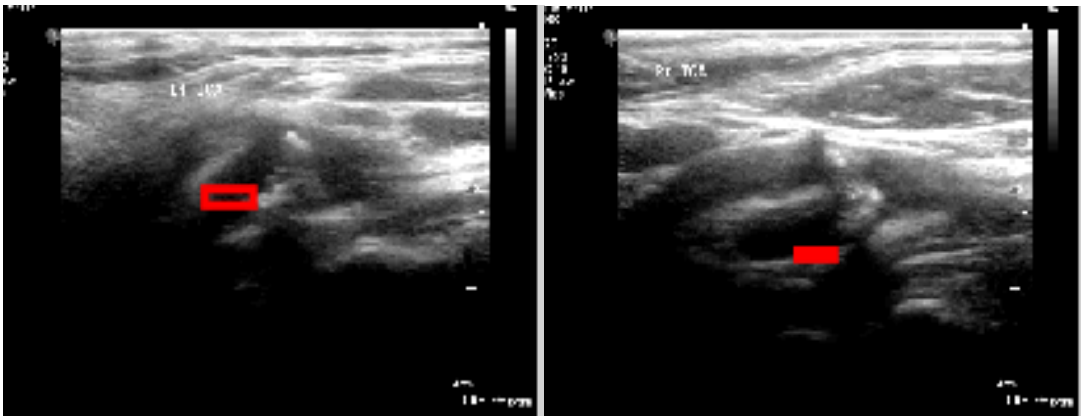

Figure 4. 11: Subject 11 – Left and Right ROI Placement.

4.3.12 Subject 12

In this case, the ROI was placed along a region directly impacted by plaque, yet kernel acceptance performance was excellent, supporting precise speckle tracking. The diameter waveform exhibited limited overall variation with a relatively flat baseline and only minor pulsatile excursions (≤0.04 mm), reflecting marked wall stiffening. The displacement trace presented a smooth multiphasic oscillation, with an early antegrade shift (~+0.02 mm) followed by subtle retrograde behavior (~−0.05 mm). Velocity values remained low but structured, rarely exceeding ±0.2 mm/s. The motion pattern retained its cyclic shape but lacked the energetic deformation typically observed in healthier

segments. These findings collectively point to a reduced mechanical response with preserved phase coordination, a hallmark of plaque-associated biomechanical restriction.

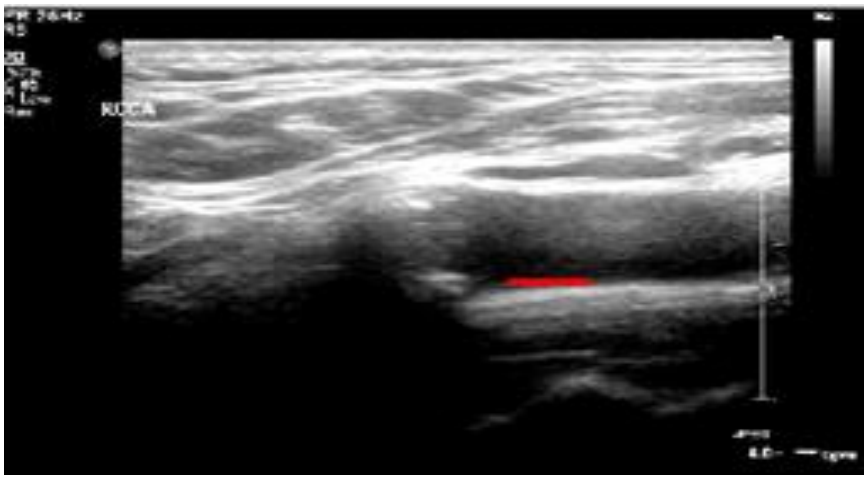

Figure 4. 12: Subject 12 – ROI placement.

4.3.13 Subject 13

Kernel acceptance remained fully stable throughout the recording. The diameter waveform demonstrated small yet clear pulsatile variations (~±0.03 mm), suggesting at least partial preservation of radial elasticity. Longitudinal displacement followed a well-recognized multiphasic CALM pattern, with antegrade movement during systole of approximately +0.03 mm and a subsequent retrograde recoil near −0.04 mm. Velocity traces were modest, largely centered around ±0.25 mm/s with smooth directional reversals. Compared with subjects whose ROIs were positioned directly on the plaque cap, the wall motion here appeared less restricted, indicating that the ROI was sufficiently distal to avoid the strongest stiffening effects while still reflecting the overall atherosclerotic burden.

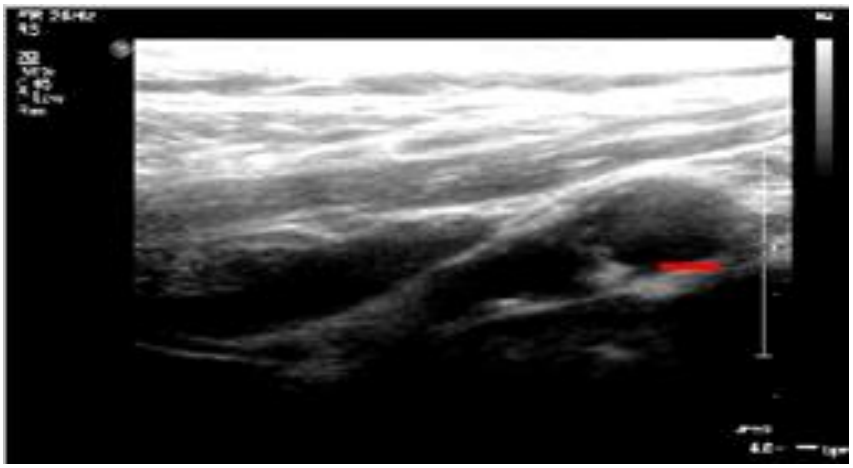

Figure 4. 13: Subject 13 – ROI placement.

4.3.14 Subject 14

For Subject 14, kernel acceptance was stable and consistently high, validating the reliability of the tracking data. The diameter waveform showed delayed and blunted outward expansion (~+0.03 mm) with more noticeable inward recoil (~−0.07 mm), indicating asymmetric compliance constraints likely imposed by eccentric plaque morphology. Longitudinal displacement followed the temporal pattern of normal CALM but with low amplitude throughout, not exceeding ±0.03 mm. Velocity peaks were similarly attenuated, remaining close to ±0.15 mm/s. Despite the preserved rhythmicity, the degree of wall mobility was substantially reduced, suggesting that plaque geometry in this region may significantly hinder longitudinal sliding between arterial layers. Nevertheless, the regularity of the movement indicates that the mechanical linkage to cardiac forces remains intact.

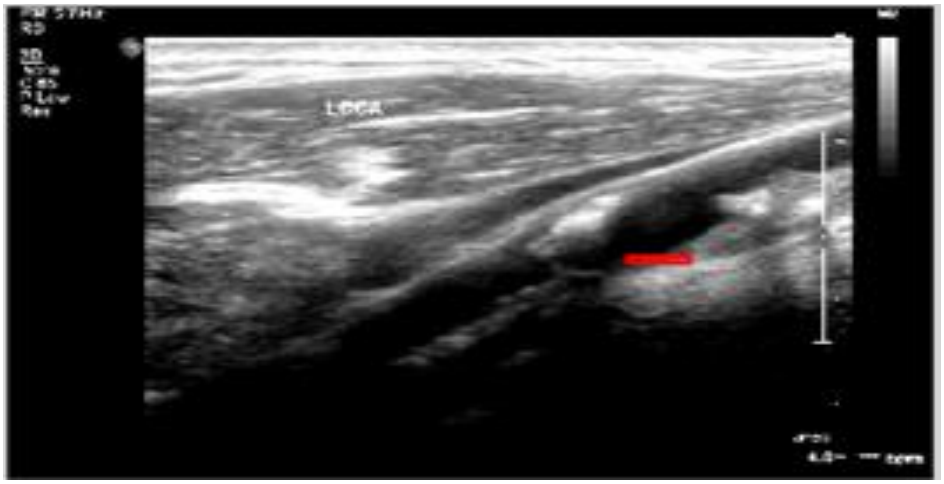

Figure 4. 14: Subject 14 – ROI placement.

4.4 Cohort-Level Interpretation

Taken together, these results demonstrate that longitudinal wall motion was preserved in morphology across all examined carotid segments, with consistent multiphasic CALM patterns observed despite the presence of plaque. However, displacement magnitudes were consistently attenuated relative to reported values in healthy arteries, supporting the interpretation that local atherosclerotic burden reduces arterial wall compliance. These findings align with previous literature describing the dampening of longitudinal wall mobility in the setting of plaque, while also showing that the fundamental oscillatory pattern of CALM remains intact.

Comprehensive graphical results, including longitudinal wall displacement, velocity, and diameter variation waveforms for all subjects, are presented in the end of this thesis.

5. Discussion

5.1 Summary of Findings

In our study we presented a custom MATLAB implementation of multiple block matching technique in order to evaluate carotid artery longitudinal wall motion adjacent to plaques. All in all, placing multiple kernels along the vessel wall provided not only stable estimates across frames but also kernel

acceptance rate showed good performance enhancing robustness. The normalized cross-correlation approach we used assisted in reliable tracking with low computational cost. Incorporation of drift removal and smoothing steps yielded physiologically plausible displacement and velocity waveforms, minimizing the impact of probe creep and noise.

Results depict multiphasic waveforms for displacement and velocity across all subjects. However, peak values of both displacement and velocity were generally reduced compared with the ones that are reported in the literature for healthy individuals. These findings are consistent with arterial stiffening and reduced compliance processes, since all eight subjects exhibit atherosclerotic plaques in their carotid arteries. Atherosclerotic disease process is chronic and involves gradual remodeling of vessels that increases wall thickness and collagen content. Reduced displacement magnitude upstream or downstream from the plaque may reflect altered wall mechanics, plaque burden or reduced elasticity. Therefore, CALM measurement could represent a functional and a novel marker for early detection of atherosclerosis and arterial wall health

5.2 Study Limitations

Certain limitations of our study should be acknowledged also. Manual placement of the ROI may introduce operator-dependent variability, which could affect reproducibility of our results across observers. The cine loops were acquired at frame rates of 35 Hz, which, while sufficient for capturing the main features of carotid wall motion, may not fully resolve rapid motion components compared with higher frame rate research ultrasound systems.

Also, ROI placement was performed manually, introducing some operator dependence. While kernel acceptance metrics suggest reliable tracking, future integration of automated segmentation could improve repeatability and facilitate larger-scale evaluation.

The number of analyzed carotid segments (n=14) and total subjects remains relatively small. Although trends were consistent across the dataset, statistical generalization would require a larger population including both disease and healthy controls to establish normative ranges for CALM.

Finally, it is relevant to note that the cine loops included both left and right carotid arteries. The anatomical distance from the heart may influence the mechanical loading of the arterial wall, with the right carotid generally experiencing slightly different hemodynamic and pressure wave reflections than the left. While this study was not designed to systematically compare side-to-side differences, acknowledging this anatomical factor adds context to the interpretation of CALM variability across subjects.

5.3 Future Directions

Building on the findings of this study, several avenues for future work can be proposed. Manual placement of the region of interest could be replaced by automated segmentation algorithms, reducing operator dependency and improving reproducibility. Moreover, future studies including larger populations with both healthy and diseased carotid arteries are of major importance in order to perform statistical comparisons and establish normative reference values for CALM. Cine loops acquired at higher frame rates would allow better temporal resolution of rapid systolic events and may reveal subtle waveform features currently missing in standard B-mode acquisitions. Finally, integrating CALM measurements with conventional vascular markers such as intima–media thickness, plaque morphology, and hemodynamic indices could help clarify the clinical role of CALM as a predictor of vascular stiffness and plaque vulnerability.

6. Conclusion

6.1 Summary of Findings

This thesis presented a custom MATLAB implementation of a multiple block-matching technique to evaluate carotid artery longitudinal wall motion (CALM) adjacent to atherosclerotic plaques. The approach demonstrated that placing multiple kernels along the vessel wall provided stable estimates of displacement across frames, while the kernel acceptance rate indicated robust tracking performance. The use of normalized cross-correlation enabled reliable motion estimation at relatively low computational cost. Furthermore, the incorporation of drift removal and smoothing steps yielded physiologically plausible displacement and velocity waveforms, reducing the influence of probe creep and noise.

The results consistently revealed multiphasic displacement and velocity waveforms across all subjects. However, the observed peak values were lower compared with reference values for healthy individuals reported in prior studies. This reduction is consistent with arterial stiffening and diminished vascular compliance, pathophysiological processes typically associated with atherosclerosis. Since all participants exhibited carotid plaques, these findings suggest that CALM measurement may serve as a sensitive functional marker of altered wall mechanics and reduced arterial elasticity.

While the study provided promising results, certain methodological constraints were identified. Tracking was performed in one dimension only, excluding radial and out-of-plane motion. Manual region-of-interest placement introduced operator dependence, and the small sample size (fourteen subjects) limited statistical generalizability. In addition, cine loops acquired at 35 Hz frame rates may not have fully resolved rapid systolic wall motion. Finally, inclusion of both left and right carotid arteries introduced anatomical variability that may influence CALM interpretation.

6.2 Final Reflections

Despite its limitations, this thesis demonstrates that CALM assessment using multiple block matching is technically feasible and clinically relevant. The reduced displacement and velocity magnitudes observed near plaques highlight the potential of CALM as an early functional marker of vascular stiffening and altered wall mechanics. Compared with conventional structural indices such as intima–media thickness or plaque morphology, CALM offers a complementary and dynamic perspective on arterial health.

Looking ahead, several avenues for advancement emerge. Extending the methodology to two-dimensional speckle tracking would provide a more comprehensive assessment of carotid wall mechanics, capturing both longitudinal and radial motion. Automation of region-of-interest placement through segmentation algorithms would reduce operator dependence and enhance reproducibility. Larger-scale studies including both healthy and diseased populations are essential for establishing normative reference values and enabling robust statistical comparisons. Moreover, acquisitions at higher frame rates could refine temporal resolution and reveal subtle waveform features currently overlooked. Integrating CALM with established vascular biomarkers may ultimately clarify its role as a predictor of stiffness, plaque vulnerability, and overall cardiovascular risk.

In broader context, this work illustrates the importance of functional vascular imaging in complementing anatomical assessment. As imaging technologies evolve, the capacity to track vessel wall dynamics may provide novel insights into disease progression and therapeutic efficacy. The methodological framework established here offers a foundation for future investigations into functional imaging markers of vascular health.

6.3 Data Availability

The cine loops, MATLAB implementation details, and resulting displacement and velocity data used in this study are available from the author upon reasonable request.

7. Bibliography

Ahlgren, Å. R., Cinthio, M., Persson, H. W., & Lindström, K. (2012). Different Patterns of Longitudinal Displacement of the Common Carotid Artery Wall in Healthy Humans Are Stable Over a Four-Month Period. *Ultrasound in Medicine & Biology*, *38*(6), 916–925. https://doi.org/10.1016/j.ultrasmedbio.2012.02.005

Ahlgren, Å. R., Cinthio, M., Steen, S., Persson, H. W., Sjöberg, T., & Lindström, K. (2009). Effects of adrenaline on longitudinal arterial wall movements and resulting intramural shear strain: A first report. *Clinical Physiology and Functional Imaging*, *29*(5), 353–359. https://doi.org/10.1111/j.1475-097X.2009.00875.x

Ahlgren, Å. R., Steen, S., Segstedt, S., Erlöv, T., Lindström, K., Sjöberg, T., Persson, H. W., Ricci, S., Tortoli, P., & Cinthio, M. (2015). Profound Increase in Longitudinal Displacements of the Porcine Carotid Artery Wall Can Take Place Independently of Wall Shear Stress: A Continuation Report. *Ultrasound in Medicine & Biology*, *41*(5), 1342–1353. https://doi.org/10.1016/j.ultrasmedbio.2015.01.005

Athaide, C. E., Spronck, B., & Au, J. S. (2022). Physiological basis for longitudinal motion of the arterial wall. *American Journal of Physiology-Heart and Circulatory Physiology*, *322*(5), H689–H701. https://doi.org/10.1152/ajpheart.00567.2021

Au, J. S., Bochnak, P. A., Valentino, S. E., Cheng, J. L., Stöhr, E. J., & MacDonald, M. J. (2018). Cardiac and haemodynamic influence on

carotid artery longitudinal wall motion. *Experimental Physiology*, *103*(1), 141–152. https://doi.org/10.1113/EP086621

Au, J. S., Ditor, D. S., MacDonald, M. J., & Stöhr, E. J. (2016). Carotid artery longitudinal wall motion is associated with local blood velocity and left ventricular rotational, but not longitudinal, mechanics. *Physiological Reports*, *4*(14), e12872. https://doi.org/10.14814/phy2.12872

Au, J. S., Proudfoot, N. A., Timmons, B. W., & MacDonald, M. J. (2019a). Retrograde shift in carotid artery longitudinal wall motion after one-year follow-up in children. *Atherosclerosis*, *288*, 26–32. https://doi.org/10.1016/j.atherosclerosis.2019.07.005

Au, J. S., Proudfoot, N. A., Timmons, B. W., & MacDonald, M. J. (2019b). Retrograde shift in carotid artery longitudinal wall motion after one-year follow-up in children. *Atherosclerosis*, *288*, 26–32. https://doi.org/10.1016/j.atherosclerosis.2019.07.005

Au, J. S., Valentino, S. E., McPhee, P. G., & MacDonald, M. J. (2017). Diastolic Carotid Artery Longitudinal Wall Motion Is Sensitive to Both Aging and Coronary Artery Disease Status Independent of Arterial Stiffness. *Ultrasound in Medicine & Biology*, *43*(9), 1906–1918. https://doi.org/10.1016/j.ultrasmedbio.2017.04.026

Cinthio, M., Ahlgren, Å. R., Bergkvist, J., Jansson, T., Persson, H. W., & Lindström, K. (2006). Longitudinal movements and resulting shear strain of the arterial wall. *American Journal of Physiology-Heart and Circulatory Physiology*, *291*(1), H394–H402. https://doi.org/10.1152/ajpheart.00988.2005

Cinthio, M., Ahlgren, A. R., Jansson, T., Eriksson, A., Persson, H. W., & Lindstrom, K. (2005). Evaluation of an ultrasonic echo-tracking method for measurements of arterial wall movements in two dimensions. *IEEE Transactions on Ultrasonics, Ferroelectrics and Frequency Control*, *52*(8), 1300–1311. https://doi.org/10.1109/TUFFC.2005.1509788

Cinthio, M., Albinsson, J., Erlöv, T., Bjarnegård, N., Länne, T., & Ahlgren, Å. R. (2018a). Longitudinal Movement of the Common Carotid Artery Wall: New Information on Cardiovascular Aging. *Ultrasound in Medicine & Biology*, *44*(11), 2283–2295. https://doi.org/10.1016/j.ultrasmedbio.2018.06.001

Cinthio, M., Albinsson, J., Erlöv, T., Bjarnegård, N., Länne, T., & Ahlgren, Å. R. (2018b). Longitudinal Movement of the Common Carotid Artery Wall: New Information on Cardiovascular Aging. *Ultrasound in Medicine & Biology*, *44*(11), 2283–2295. https://doi.org/10.1016/j.ultrasmedbio.2018.06.001

Fukui, T., Parker, K. H., Imai, Y., Tsubota, K., Ishikawa, T., Wada, S., & Yamaguchi, T. (2007). Effect of Wall Motion on Arterial Wall Shear Stress. *Journal of Biomechanical Science and Engineering*, *2*(2), 58–68. https://doi.org/10.1299/jbse.2.58

Gastounioti, A., Golemati, S., Stoitsis, J., & Nikita, K. S. (2011). Comparison of Kalman-filter-based approaches for block matching in arterial wall motion analysis from B-mode ultrasound. *Measurement Science and Technology*, *22*(11), 114008. https://doi.org/10.1088/0957-0233/22/11/114008

Gastounioti, A., Golemati, S., Stoitsis, J. S., & Nikita, K. S. (2013). Carotid artery wall motion analysis from B-mode ultrasound using adaptive block matching: *In silico* evaluation and *in vivo* application. *Physics in Medicine and Biology*, *58*(24), 8647–8661. https://doi.org/10.1088/0031-9155/58/24/8647

Gastounioti, A., Kolias, V., Golemati, S., Tsiaparas, N. N., Matsakou, A., Stoitsis, J. S., Kadoglou, N. P. E., Gkekas, C., Kakisis, J. D., Liapis, C. D., Karakitsos, P., Sarafis, I., Angelidis, P., & Nikita, K. S. (2014). CAROTID – A web-based platform for optimal personalized management of atherosclerotic patients. *Computer Methods and Programs in Biomedicine*, *114*(2), 183–193. https://doi.org/10.1016/j.cmpb.2014.02.006

Gepner, A. D., Colangelo, L. A., Reilly, N., Korcarz, C. E., Kaufman, J. D., & Stein, J. H. (2015). Carotid Artery Longitudinal Displacement, Cardiovascular Disease and Risk Factors: The Multi-Ethnic Study of Atherosclerosis. *PLOS ONE*, *10*(11), e0142138. https://doi.org/10.1371/journal.pone.0142138

Gepner, A. D., McClelland, R. L., Korcarz, C. E., Young, R., Kaufman, J. D., Mitchell, C. C., & Stein, J. H. (2019). Carotid artery displacement and cardiovascular disease risk in the Multi-Ethnic Study of Atherosclerosis. *Vascular Medicine*, *24*(5), 405–413. https://doi.org/10.1177/1358863X19853362

Golemati, S., Sassano, A., Lever, M. J., Bharath, A. A., Dhanjil, S., & Nicolaides, A. N. (2003). Carotid artery wall motion estimated from b-mode ultrasound using region tracking and block matching. *Ultrasound*

in Medicine & Biology, *29*(3), 387–399. https://doi.org/10.1016/S0301-5629(02)00760-3

Persson, M., Rydén Ahlgren, Å., Jansson, T., Eriksson, A., Persson, H. W., & Lindström, K. (2003). A new non-invasive ultrasonic method for simultaneous measurements of longitudinal and radial arterial wall movements: First *in vivo* trial. *Clinical Physiology and Functional Imaging*, *23*(5), 247–251. https://doi.org/10.1046/j.1475-097X.2003.00504.x

Proudfoot, N. A., Au, J. S., Timmons, B. W., & MacDonald, M. J. (2019). Associations between carotid artery longitudinal wall motion and arterial stiffness indicators in young children. *Atherosclerosis*, *287*, 64–69. https://doi.org/10.1016/j.atherosclerosis.2019.06.895

Rizi, F. Y., Au, J., Yli-Ollila, H., Golemati, S., Makūnaitė, M., Orkisz, M., Navab, N., MacDonald, M., Laitinen, T. M., Behnam, H., Gao, Z., Gastounioti, A., Jurkonis, R., Vray, D., Laitinen, T., Sérusclat, A., Nikita, K. S., & Zahnd, G. (2020). Carotid Wall Longitudinal Motion in Ultrasound Imaging: An Expert Consensus Review. *Ultrasound in Medicine & Biology*, *46*(10), 2605–2624. https://doi.org/10.1016/j.ultrasmedbio.2020.06.006

Svedlund, S., & Gan, L. (2011). Longitudinal wall motion of the common carotid artery can be assessed by velocity vector imaging. *Clinical Physiology and Functional Imaging*, *31*(1), 32–38. https://doi.org/10.1111/j.1475-097X.2010.00976.x

Taivainen, S. H., Yli-Ollila, H., Juonala, M., Kähönen, M., Raitakari, O. T., Laitinen, T. M., & Laitinen, T. P. (2017). Interrelationships between

indices of longitudinal movement of the common carotid artery wall and the conventional measures of subclinical arteriosclerosis. *Clinical Physiology and Functional Imaging*, *37*(3), 305–313. https://doi.org/10.1111/cpf.12305

Taivainen, S. H., Yli-Ollila, H., Juonala, M., Kähönen, M., Raitakari, O. T., Laitinen, T. M., & Laitinen, T. P. (2018). Influence of cardiovascular risk factors on longitudinal motion of the common carotid artery wall. *Atherosclerosis*, *272*, 54–59. https://doi.org/10.1016/j.atherosclerosis.2018.02.037

Tat, J., Au, J. S., Keir, P. J., & MacDonald, M. J. (2017). Reduced common carotid artery longitudinal wall motion and intramural shear strain in individuals with elevated cardiovascular disease risk using speckle tracking. *Clinical Physiology and Functional Imaging*, *37*(2), 106–116. https://doi.org/10.1111/cpf.12270

Yli-Ollila, H., Laitinen, T., Weckström, M., & Laitinen, T. M. (2013). Axial and Radial Waveforms in Common Carotid Artery: An Advanced Method for Studying Arterial Elastic Properties in Ultrasound Imaging. *Ultrasound in Medicine & Biology*, *39*(7), 1168–1177. https://doi.org/10.1016/j.ultrasmedbio.2013.01.018

Yli-Ollila, H., Tarvainen, M. P., Laitinen, T. P., & Laitinen, T. M. (2016). Principal Component Analysis of the Longitudinal Carotid Wall Motion in Association with Vascular Stiffness: A Pilot Study. *Ultrasound in Medicine & Biology*, *42*(12), 2873–2886. https://doi.org/10.1016/j.ultrasmedbio.2016.07.020

Zahnd, G., Balocco, S., Sérusclat, A., Moulin, P., Orkisz, M., & Vray, D. (2015a). Progressive Attenuation of the Longitudinal Kinetics in the Common Carotid Artery: Preliminary in Vivo Assessment. *Ultrasound in Medicine & Biology*, *41*(1), 339–345. https://doi.org/10.1016/j.ultrasmedbio.2014.07.019

Zahnd, G., Balocco, S., Sérusclat, A., Moulin, P., Orkisz, M., & Vray, D. (2015b). Progressive Attenuation of the Longitudinal Kinetics in the Common Carotid Artery: Preliminary in Vivo Assessment. *Ultrasound in Medicine & Biology*, *41*(1), 339–345. https://doi.org/10.1016/j.ultrasmedbio.2014.07.019

Zahnd, G., Boussel, L., Serusclat, A., & Vray, D. (2011). Intramural shear strain can highlight the presence of atherosclerosis: A clinical in vivo study. *2011 IEEE International Ultrasonics Symposium*, 1770–1773. https://doi.org/10.1109/ULTSYM.2011.0442

Zahnd, G., Kapellas, K., Van Hattem, M., Van Dijk, A., Sérusclat, A., Moulin, P., Van Der Lugt, A., Skilton, M., & Orkisz, M. (2017). A Fully-Automatic Method to Segment the Carotid Artery Layers in Ultrasound Imaging: Application to Quantify the Compression-Decompression Pattern of the Intima-Media Complex During the Cardiac Cycle. *Ultrasound in Medicine & Biology*, *43*(1), 239–257. https://doi.org/10.1016/j.ultrasmedbio.2016.08.016

Zahnd, G., Orkisz, M., Sérusclat, A., Moulin, P., & Vray, D. (2013). Evaluation of a Kalman-based block matching method to assess the bi-dimensional motion of the carotid artery wall in B-mode ultrasound

sequences. *Medical Image Analysis*, *17*(5), 573–585. https://doi.org/10.1016/j.media.2013.03.006

Zahnd, G., Saito, K., Nagatsuka, K., Otake, Y., & Sato, Y. (2018). Dynamic Block Matching to assess the longitudinal component of the dense motion field of the carotid artery wall in B-mode ultrasound sequences—Association with coronary artery disease. *Medical Physics*, *45*(11), 5041–5053. https://doi.org/10.1002/mp.13186

Zahnd, G., Vray, D., Sérusclat, A., Alibay, D., Bartold, M., Brown, A., Durand, M., Jamieson, L. M., Kapellas, K., Maple-Brown, L. J., O'Dea, K., Moulin, P., Celermajer, D. S., & Skilton, M. R. (2012a). Longitudinal Displacement of the Carotid Wall and Cardiovascular Risk Factors: Associations with Aging, Adiposity, Blood Pressure and Periodontal Disease Independent of Cross-Sectional Distensibility and Intima-Media Thickness. *Ultrasound in Medicine & Biology*, *38*(10), 1705–1715. https://doi.org/10.1016/j.ultrasmedbio.2012.05.004

Zahnd, G., Vray, D., Sérusclat, A., Alibay, D., Bartold, M., Brown, A., Durand, M., Jamieson, L. M., Kapellas, K., Maple-Brown, L. J., O'Dea, K., Moulin, P., Celermajer, D. S., & Skilton, M. R. (2012b). Longitudinal Displacement of the Carotid Wall and Cardiovascular Risk Factors: Associations with Aging, Adiposity, Blood Pressure and Periodontal Disease Independent of Cross-Sectional Distensibility and Intima-Media Thickness. *Ultrasound in Medicine & Biology*, *38*(10), 1705–1715. https://doi.org/10.1016/j.ultrasmedbio.2012.05.004

8 Appendices

8.1 Source Code (MATLAB)

```
% carotid_LWM_video.m
% Carotid longitudinal wall motion + diameter waveform from a B-mode *video*
% - Longitudinal motion (X): 1-D NCC across thin FAR-wall band
% - Diameter (Y): 1-D NCC across thin bands at NEAR and FAR walls
%
% Ready to run: draws 3 ROIs on the first frame and processes the whole clip.

%% ================ USER SETTINGS ============================
videoPath       = "s1ricaplq.avi";   % <- your video (mp4/avi/mov) or multi-frame DICOM (.dcm)
fps_manual      = 35;                % used only if FPS can't be read from file
mm_per_pixel    = 0.0718;            % mm/px in X; if anisotropic, set Y separately below
outTag          = "subject1";
streamingMode   = true;              % true=reads one frame at a time (low RAM); false=load all frames

% Tracking params (longitudinal X)
kw = 40; kh = 10; stride = 12; S = 10; ncc_min = 0.65; mad_k = 2.5;

% Smoothing / drift (applied to displacement, velocity, and diameter)
useSavGol = true; sgolay_window = 11; sgolay_poly = 2;
removeDrift = true; drift_window_sec = 1.5;

% ===== Diameter (Y-tracking) params =====
mm_per_pixel_y  = mm_per_pixel; % set separately if Y differs (anisotropic scaling)
Sy              = 8;            % vertical search half-range (px) per frame
kw_diam         = 20;           % wall kernel width in X (px)
kh_wall         = 6;            % wall kernel height in Y (px)
stride_diam     = 12;           % stride in X for placing wall kernels
ncc_min_y       = 0.65;         % NCC threshold for Y tracking
mad_k_y         = 2.5;          % MAD-based outlier factor

%% ================ LOAD VIDEO ============================
assert(isfile(videoPath), 'File not found: %s', videoPath);
[framesReader, fps, N, firstFrame, streamingMode] = open_video_any(videoPath, fps_manual, streamingMode);
[nrows, ncols] = size(firstFrame);

%% ================ PICK ROIs (once) ======================
figure('Name','FAR wall band for longitudinal X (thin horizontal rectangle)');
imshow(firstFrame,[], "InitialMagnification","fit");
```

```
title('Draw thin horizontal rectangle across the FAR wall (longitudinal X). Double-click to confirm.');
roi = drawrectangle('StripeColor','r'); customWait(roi);
rect = round(roi.Position); close(gcf);
rect = clamp_rect(rect, ncols, nrows);

figure('Name','NEAR wall band (diameter Y)');
imshow(firstFrame,[], "InitialMagnification","fit");
title('Draw thin horizontal rectangle on the NEAR wall. Double-click to confirm.');
roiN = drawrectangle('StripeColor','y'); customWait(roiN);
nearRect = round(roiN.Position); close(gcf);
nearRect = clamp_rect(nearRect, ncols, nrows);

figure('Name','FAR wall band (diameter Y)');
imshow(firstFrame,[], "InitialMagnification","fit");
title('Draw thin horizontal rectangle on the FAR wall. Double-click to confirm.');
roiF = drawrectangle('StripeColor','c'); customWait(roiF);
farRect = round(roiF.Position); close(gcf);
farRect = clamp_rect(farRect, ncols, nrows);

%% ========== TILE KERNELS (X for LWM, Y for Diameter) ====================
kernels = make_kernels(rect, kw, kh, stride, ncols, nrows);
assert(~isempty(kernels), 'No kernels for longitudinal X. Make ROI wider or reduce kw.');

nearK = make_vertical_kernels(nearRect, kw_diam, kh_wall, stride_diam, ncols, nrows);
farK  = make_vertical_kernels(farRect,  kw_diam, kh_wall, stride_diam, ncols, nrows);
assert(~isempty(nearK) && ~isempty(farK), 'No near/far wall kernels. Adjust ROIs or kw_diam.');

%% ======= EXPORT ROI/KERNEL SPEC (to reuse in other pipeline) ============
roiSpec = struct();
roiSpec.videoPath       = videoPath;
roiSpec.outTag          = outTag;
roiSpec.frame0_size     = [nrows, ncols];
roiSpec.fps             = fps;
roiSpec.mm_per_pixel_x  = mm_per_pixel;
roiSpec.mm_per_pixel_y  = mm_per_pixel_y;

% store raw rectangles (MATLAB [x y w h] in pixels)
roiSpec.rect_longitudinal = rect;
roiSpec.rect_near         = nearRect;
roiSpec.rect_far          = farRect;

% store kernels as Nx4 [x y w h]
toArray = @(K) reshape([[K.x]; [K.y]; [K.w]; [K.h]]', [], 4);
```

```
roiSpec.kernels_longitudinal = toArray(kernels);
roiSpec.kernels_near         = toArray(nearK);
roiSpec.kernels_far          = toArray(farK);

% save both .mat (lossless) and .json (portable)
outDir = fullfile(fileparts(videoPath), "lwm_outputs");
if ~exist(outDir,'dir'), mkdir(outDir); end
save(fullfile(outDir, sprintf('ROIS_%s.mat', outTag)), 'roiSpec');

try
    jsonStr = jsonencode(roiSpec);
    fid = fopen(fullfile(outDir, sprintf('ROIS_%s.json', outTag)),'w');
    fwrite(fid, jsonStr, 'char'); fclose(fid);
catch
    % jsonencode not available in very old MATLAB; .mat is fine.
end

%% ========== STREAMING OR BULK PROCESSING SETUP ==========================
M_drift = max(3, round(drift_window_sec * fps));

% Pre-allocate small when N known; otherwise grow vectors safely
perFrameShift = zeros(0,1,'single');
accRate       = zeros(0,1,'single');
yNear         = zeros(0,1,'single');
yFar          = zeros(0,1,'single');

% Initial absolute Y positions (kernel tops) for diameter tracking
yNear(1,1) = median(arrayfun(@(rk) rk.y, nearK),'omitnan');
yFar(1,1)  = median(arrayfun(@(rk) rk.y,  farK),'omitnan');

%% ========== MAIN TRACKING LOOP ========================================
fprintf('Processing %d frames at %.3f fps...\n', N, fps);
tStart = tic;

if ~streamingMode
    % ---- Bulk read (may use more RAM) ----
    frames = read_all_frames(framesReader, N);
    % Iterate frame-to-frame
    for t = 1:(size(frames,3)-1)
        I0 = frames(:,:,t);
        I1 = frames(:,:,t+1);
        [dX, acceptPct, kernels] = track_longitudinal_X(I0, I1, kernels, S, ncc_min, mad_k, ncols);
        [yN, nearK]              = track_vertical_band(I0, I1, nearK, Sy, ncc_min_y, mad_k_y, nrows);
        [yF, farK]               = track_vertical_band(I0, I1, farK,  Sy, ncc_min_y, mad_k_y, nrows);
```

```
        perFrameShift(end+1,1) = dX;
        accRate(end+1,1)       = acceptPct;
        yNear(end+1,1)         = yN;
        yFar(end+1,1)          = yF;
    end
else
    % ---- Streaming (low RAM) ----
    I0 = firstFrame;
    for t = 1:(N-1)
        I1 = read_next_frame(framesReader);
        if isempty(I1), break; end

        [dX, acceptPct, kernels] = track_longitudinal_X(I0, I1, kernels, S, ncc_min,
mad_k, ncols);
        [yN, nearK]                = track_vertical_band(I0, I1, nearK, Sy, ncc_min_y,
mad_k_y, nrows);
        [yF, farK]                 = track_vertical_band(I0, I1, farK,  Sy, ncc_min_y, mad_k_y,
nrows);

        perFrameShift(end+1,1) = dX;
        accRate(end+1,1)       = acceptPct;
        yNear(end+1,1)         = yN;
        yFar(end+1,1)          = yF;

        I0 = I1; % advance
    end
end

procTime = toc(tStart);
fprintf('Done in %.2f s. Effective frames processed: %d\n', procTime,
numel(perFrameShift)+1);

%% ========== DISPLACEMENT & VELOCITY
====================================
cum_disp_px = cumsum(perFrameShift);
cum_disp_mm = cum_disp_px * mm_per_pixel;

if removeDrift
    if exist('movmedian','file')==2
        trend = movmedian(cum_disp_mm, M_drift);
    else
        trend = detrend(cum_disp_mm,'linear');
    end
    cum_disp_driftless = cum_disp_mm - trend;
else
    cum_disp_driftless = cum_disp_mm;
end
```

```
dt = 1 / fps;
vel_mm_s = [diff(cum_disp_driftless)./dt; 0];

% Savitzkyβ€“Golay or median smoothing
if useSavGol && exist('sgolayfilt','file')==2
    w = sgolay_window;
    if mod(w,2)==0, w = w + 1; end
    if w <= sgolay_poly, w = sgolay_poly + 3; end
    if mod(w,2)==0, w = w + 1; end
    cum_disp_sm = sgolayfilt(double(cum_disp_driftless), sgolay_poly, w);
    vel_sm      = sgolayfilt(double(vel_mm_s),          sgolay_poly, w);
else
    w = max(3, sgolay_window);
    if exist('movmedian','file')==2
        cum_disp_sm = movmedian(cum_disp_driftless, w);
        vel_sm      = movmedian(vel_mm_s,          w);
    else
        cum_disp_sm = cum_disp_driftless;
        vel_sm      = vel_mm_s;
    end
end

%% ========== DIAMETER & DISTENSION VELOCITY ============================
% yNear / yFar contain absolute kernel top rows per frame (length == number of frames)
% Diameter uses per-frame NEAR vs FAR distance (pixels)
diam_px = (yFar - yNear);
diam_mm = diam_px * mm_per_pixel_y;

if removeDrift
    if exist('movmedian','file')==2
        trendD = movmedian(diam_mm, M_drift);
    else
        trendD = detrend(diam_mm,'linear');
    end
    diam_driftless = diam_mm - trendD;
else
    diam_driftless = diam_mm;
end

dv_mm_s = [diff(diam_driftless) ./ dt; 0];

if useSavGol && exist('sgolayfilt','file')==2
    w = sgolay_window;
    if mod(w,2)==0, w = w + 1; end
    if w <= sgolay_poly, w = sgolay_poly + 3; end
    if mod(w,2)==0, w = w + 1; end
    diam_sm = sgolayfilt(double(diam_driftless), sgolay_poly, w);
```

```
    dv_sm   = sgolayfilt(double(dv_mm_s),       sgolay_poly, w);
else
    w = max(3, sgolay_window);
    if exist('movmedian','file')==2
        diam_sm = movmedian(diam_driftless, w);
        dv_sm   = movmedian(dv_mm_s,       w);
    else
        diam_sm = diam_driftless;
        dv_sm   = dv_mm_s;
    end
end

%%                                          ==========                                          PLOTS
=====================================================
applyAxes = @(ax) set(ax, ...
    'Color','w', 'XColor','k', 'YColor','k', ...
    'LineWidth',1.5, 'FontSize',16, 'FontName','Arial', ...
    'GridColor',[0.85 0.85 0.85], 'GridAlpha',1);

titleFmt  = @(s) title(s,'Color','k','FontWeight','bold','FontSize',20);
labelFmtX = @(s) xlabel(s,'Color','k','FontWeight','bold');
labelFmtY = @(s) ylabel(s,'Color','k','FontWeight','bold');

% convenient time vectors
t_disp = (1:numel(cum_disp_sm))/fps;
t_diam = (1:numel(diam_sm))/fps;

% ---- Figure A: ROI & kernels (3 panels)
figA = figure('Name','ROI & kernels','Color','w','Position',[100 100 1200 600]);
tiledlayout(figA,1,3,'Padding','compact','TileSpacing','compact');

nexttile; imshow(firstFrame,[], "InitialMagnification","fit"); hold on;
rectangle('Position',rect,'EdgeColor','r','LineWidth',2); hold off;
titleFmt('Longitudinal ROI (red)'); applyAxes(gca);

nexttile; imshow(firstFrame,[], "InitialMagnification","fit"); hold on;
rectangle('Position',nearRect,'EdgeColor','y','LineWidth',2);
for k = 1:numel(nearK), r = nearK(k); rectangle('Position',[r.x r.y r.w
r.h],'EdgeColor','g','LineWidth',1); end
hold off; titleFmt('NEAR wall ROI (yellow) & kernels'); applyAxes(gca);

nexttile; imshow(firstFrame,[], "InitialMagnification","fit"); hold on;
rectangle('Position',farRect,'EdgeColor','c','LineWidth',2);
for k = 1:numel(farK), r = farK(k); rectangle('Position',[r.x r.y r.w
r.h],'EdgeColor','m','LineWidth',1); end
hold off; titleFmt('FAR wall ROI (cyan) & kernels'); applyAxes(gca);

% ---- Figure B: ROI (red) vs Kernels (2 large panels) ----
figB = figure('Name','ROI and Kernels (wide)','Color','w','Position',[100 100 1400 650]);
```

```
tiledlayout(figB,1,2,'Padding','compact','TileSpacing','compact');

nexttile; imshow(firstFrame,[], "InitialMagnification","fit"); hold on;
rectangle('Position',rect,'EdgeColor','r','LineWidth',2); hold off;
titleFmt('ROI (red)'); applyAxes(gca);

nexttile; imshow(firstFrame,[], "InitialMagnification","fit"); hold on;
rectangle('Position',nearRect,'EdgeColor','y','LineWidth',2);
for k = 1:numel(nearK), r = nearK(k); rectangle('Position',[r.x r.y r.w
r.h],'EdgeColor','g','LineWidth',1); end
rectangle('Position',farRect,'EdgeColor','c','LineWidth',2);
for k = 1:numel(farK), r = farK(k); rectangle('Position',[r.x r.y r.w
r.h],'EdgeColor','m','LineWidth',1); end
hold off; titleFmt('Kernels'); applyAxes(gca);

% ---- Figure C: Displacement & Velocity (stacked) ----
figC = figure('Name','Displacement and Velocity','Color','w','Position',[120 120 1280
720]);
tiledlayout(figC,2,1,'Padding','compact','TileSpacing','compact');

nexttile;
plot(t_disp, cum_disp_sm, 'k','LineWidth',2.5); grid on; applyAxes(gca);
labelFmtX('Time (s)'); labelFmtY('Displacement (mm)'); titleFmt('Longitudinal
displacement (smoothed)');

nexttile;
plot(t_disp, vel_sm, 'k','LineWidth',2.5); grid on; applyAxes(gca);
labelFmtX('Time (s)'); labelFmtY('Velocity (mm/s)'); titleFmt('Velocity (smoothed)');

% ---- Figure D: Diameter & Distension velocity (stacked) ----
figD = figure('Name','Diameter waveform','Color','w','Position',[140 140 1500 750]);
tiledlayout(figD,2,1,'Padding','compact','TileSpacing','compact');

nexttile;
plot(t_diam, diam_sm, 'k','LineWidth',2.5); grid on; applyAxes(gca);
labelFmtX('Time (s)'); labelFmtY('Diameter (mm)'); titleFmt('Carotid diameter
(smoothed)');

nexttile;
plot(t_diam, dv_sm, 'k','LineWidth',2.0); grid on; applyAxes(gca);
labelFmtX('Time (s)'); labelFmtY('Distension velocity (mm/s)'); titleFmt('Diameter
change rate (smoothed)');

% ---- Figure E: Kernel acceptance rate (wide, single axis) ----
figE = figure('Name','Kernel acceptance rate','Color','w','Position',[160 160 1200 420]);
plot((1:numel(accRate))/fps, accRate, 'k','LineWidth',2.5);
grid on; applyAxes(gca);
labelFmtX('Time (s)'); labelFmtY('Accepted kernels (%)'); titleFmt('Kernel acceptance
rate');
```

```
ylim([0 100]);

%% ========== SAVE OUTPUTS ==========
[baseFolder, ~, ~] = fileparts(videoPath);
if isempty(baseFolder), baseFolder = "."; end
outDir = fullfile(baseFolder, "lwm_outputs");
if ~exist(outDir, 'dir'); mkdir(outDir); end

% Align lengths to #pairs = (#frames-1)
M = numel(perFrameShift);
T = table((1:M)', ((1:M)')/fps, ...
        cum_disp_sm(1:M), vel_sm(1:M), accRate(1:M), ...
        diam_sm(1:M),     dv_sm(1:M), ...
    'VariableNames',
{'Frame','Time_s','Disp_mm','Vel_mm_s','Accept_pct','Diam_mm','DistVel_mm_s'});

writetable(T, fullfile(outDir, sprintf('LWM_%s.csv', outTag)));

% Save figures with correct handles
saveas(figC, fullfile(outDir, sprintf('LWM_%s_disp_vel.png', outTag)));
saveas(figE, fullfile(outDir, sprintf('LWM_%s_accept.png',   outTag)));
saveas(figB, fullfile(outDir, sprintf('LWM_%s_rois.png',     outTag))); % wide ROIs & kernels
saveas(figD, fullfile(outDir, sprintf('LWM_%s_diameter.png', outTag)));

% Optional vector PDF exports:
% exportgraphics(figC, fullfile(outDir, sprintf('LWM_%s_disp_vel.pdf', outTag)), 'ContentType','vector');
% exportgraphics(figE, fullfile(outDir, sprintf('LWM_%s_accept.pdf',   outTag)), 'ContentType','vector');
% exportgraphics(figB, fullfile(outDir, sprintf('LWM_%s_rois.pdf',     outTag)), 'ContentType','vector');
% exportgraphics(figD, fullfile(outDir, sprintf('LWM_%s_diameter.pdf', outTag)), 'ContentType','vector');

fprintf('\nSaved outputs to: %s\n', outDir);

%% ========== LOCAL FUNCTIONS ==========
function [reader, fps, N, firstFrame, streaming] = open_video_any(pathStr, fps_manual, streaming)
    % NOTE: For DICOM, streaming is auto-disabled (bulk path used).
    [~,~,ext] = fileparts(pathStr);
    if strcmpi(ext,'.dcm')
        info = dicominfo(pathStr);
        F = dicomread(info);          % size: rows x cols x 1 x N  OR rows x cols x N
        F = squeeze(F);
        if ndims(F)==3
```

```
            if size(F,3)==3 && size(F,1)>8    % RGB multi-frame (rare)
                error('Unexpected RGB multi-frame DICOM shape.');
            end
            N = size(F,3);
            firstFrame = im2single(to_gray(F(:,:,1)));
            fps = dicom_fps(info, fps_manual);
            reader = struct('mode','dicom','buf',F,'idx',1); %#ok<STRNU>
            if streaming
                warning('Streaming disabled for DICOM; using bulk read for reliability.');
                streaming = false;
            end
        else
            error('Unsupported DICOM dimensions.');
        end
    else
        v = VideoReader(pathStr);
        fps = v.FrameRate; if isempty(fps) || ~isfinite(fps), fps = fps_manual; end
        firstFrame = im2single(to_gray(readFrame(v)));
        % Approximate N; NumFrames can be unreliable, but if present use it
        if ~isempty(v.NumFrames) && isfinite(v.NumFrames)
            N = v.NumFrames;
        else
            % Estimate frames from duration
            N = max(2, round(v.Duration * fps));
        end
        if streaming
            reader = struct('mode','videoreader','vr',v);
        else
            % rewind for bulk read
            reader = struct('mode','videoreader','vr',VideoReader(pathStr));
        end
    end
end

function fps = dicom_fps(info, fps_manual)
    fps = NaN;
    if isfield(info,'CineRate') && ~isempty(info.CineRate)
        fps = double(info.CineRate);
    elseif isfield(info,'FrameTime') && ~isempty(info.FrameTime)
        % FrameTime in ms
        fps = 1000 / double(info.FrameTime);
    end
    if isempty(fps) || ~isfinite(fps) || fps<=0
        fps = fps_manual;
    end
end

function frames = read_all_frames(reader, N)
    switch reader.mode
```

```
        case 'dicom'
            F = reader.buf;
            frames = zeros(size(F,1), size(F,2), N, 'single');
            for i=1:N
                frames(:,:,i) = im2single(to_gray(F(:,:,i)));
            end
        case 'videoreader'
            v = reader.vr;
            frames = zeros(v.Height, v.Width, N, 'single');
            i = 1;
            while hasFrame(v) && i<=N
                frames(:,:,i) = im2single(to_gray(readFrame(v)));
                i = i + 1;
            end
            frames = frames(:,:,1:i-1);
        otherwise
            error('Unknown reader mode.');
    end
end

function I = read_next_frame(reader)
    switch reader.mode
        case 'dicom'
            % DICOM "streaming" not supported by design (we auto-disabled it).
            I = [];
        case 'videoreader'
            if hasFrame(reader.vr)
                I = im2single(to_gray(readFrame(reader.vr)));
            else
                I = [];
            end
        otherwise
            I = [];
    end
end

function rect = clamp_rect(rect, ncols, nrows)
    rect(1) = max(1, rect(1)); rect(2) = max(1, rect(2));
    rect(3) = min(rect(3), ncols - rect(1));
    rect(4) = min(rect(4), nrows - rect(2));
end

function [dX, acceptPct, kernelsOut] = track_longitudinal_X(I0, I1, kernelsIn, S,
ncc_min, mad_k, ncols)
    kernels = kernelsIn;
    shifts = nan(numel(kernels),1,'single');
    scores = nan(numel(kernels),1,'single');
    for k = 1:numel(kernels)
        r = kernels(k);
```

```
        T = I0(r.y:(r.y+r.h-1), r.x:(r.x+r.w-1));
        xs = max(1, r.x - S);
        xe = min(ncols - r.w + 1, r.x + S);
        nShifts = xe - xs + 1; if nShifts < 3, continue; end
        ncc_curve = zeros(1, nShifts, 'single');
        for xi = 1:nShifts
            x_cur = xs + xi - 1;
            P = I1(r.y:(r.y+r.h-1), x_cur:(x_cur+r.w-1));
            ncc_curve(xi) = ncc_scalar(T, P);
        end
        [scoreMax, idxMax] = max(ncc_curve);
        if idxMax==1 || idxMax==nShifts
            d_sub = (xs + idxMax - 1) - r.x;
        else
            d_sub = subpixel_quadratic(ncc_curve, idxMax) + (xs + idxMax - 1) - r.x;
        end
        shifts(k) = d_sub; scores(k) = scoreMax;
        kernels(k).x = clamp(round(kernels(k).x + d_sub), 1, ncols - r.w + 1);
    end
    good = scores > ncc_min & ~isnan(shifts);
    sGood = shifts(good);
    if numel(sGood) >= 3
        medS = median(sGood); MAD = median(abs(sGood - medS));
        if MAD==0
            keep = good;
        else
            keep = false(size(shifts));
            keep(good) = abs(sGood - medS) <= mad_k * 1.4826 * MAD;
        end
    else
        keep = good;
    end
    acceptPct = 100 * sum(keep) / numel(kernels);
    dX = single(any(keep)) * median(shifts(keep),'omitnan');
    kernelsOut = kernels;
end

function [yMed, kernelsOut] = track_vertical_band(I0, I1, kernelsIn, Sy, ncc_min,
mad_k, nrows)
    kernels = kernelsIn;
    yShifts = nan(numel(kernels),1,'single');
    yScores = nan(numel(kernels),1,'single');
    for k = 1:numel(kernels)
        r = kernels(k);
        T = I0(r.y:(r.y+r.h-1), r.x:(r.x+r.w-1));
        ys = max(1, r.y - Sy);
        ye = min(nrows - r.h + 1, r.y + Sy);
        nSh = ye - ys + 1; if nSh < 3, continue; end
        ncc_curve = zeros(1, nSh, 'single');
```

```
        for yi = 1:nSh
            y_cur = ys + yi - 1;
            P = I1(y_cur:(y_cur+r.h-1), r.x:(r.x+r.w-1));
            ncc_curve(yi) = ncc_scalar(T, P);
        end
        [scoreMax, idxMax] = max(ncc_curve);
        if idxMax==1 || idxMax==nSh
            d_sub = (ys + idxMax - 1) - r.y;
        else
            d_sub = subpixel_quadratic(ncc_curve, idxMax) + (ys + idxMax - 1) - r.y;
        end
        yShifts(k) = d_sub; yScores(k) = scoreMax;
        kernels(k).y = clamp(round(kernels(k).y + d_sub), 1, nrows - r.h + 1);
    end
    good = yScores > ncc_min & ~isnan(yShifts);
    s = yShifts(good);
    if numel(s) >= 3
        med = median(s); MAD = median(abs(s - med));
        if MAD==0
            keep = good;
        else
            keep = false(size(yShifts));
            keep(good) = abs(s - med) <= mad_k * 1.4826 * MAD;
        end
    else
        keep = good;
    end
    if any(keep)
        yMed = median(arrayfun(@(rk) rk.y, kernels(keep)),'omitnan');
    else
        % Fallback: use unfiltered median (prevents NaNs from propagating)
        yMed = median(arrayfun(@(rk) rk.y, kernels),'omitnan');
    end
    kernelsOut = kernels;
end

function Igray = to_gray(I)
    I = squeeze(I);
    if ndims(I)==2
        Igray = I;
    elseif ndims(I)==3
        if size(I,3)==4, Igray = rgb2gray(I(:,:,1:3));
        else, Igray = rgb2gray(I);
        end
    else
        error('Unsupported frame dimensions.');
    end
end
```

```
function r = clamp(x,a,b), r = min(max(x,a), b); end

function [kernels] = make_kernels(rect, kw, kh, stride, ncols, nrows)
    x0 = rect(1); y0 = rect(2); W = rect(3); H = rect(4);
    xs = x0:stride:(x0 + W - kw);
    ys = y0 + round((H - kh)/2);
    ys = clamp(ys, 1, nrows - kh + 1);
    kernels = struct('x',{},'y',{},'w',{},'h',{});
    for x = xs
        k.x = clamp(round(x), 1, ncols - kw + 1);
        k.y = ys; k.w = kw; k.h = kh;
        kernels(end+1) = k; %#ok<AGROW>
    end
end

function kernels = make_vertical_kernels(rect, kw, kh, stride, ncols, nrows)
    x0 = rect(1); y0 = rect(2); W = rect(3); H = rect(4);
    xs = x0:stride:(x0 + W - kw);
    y  = y0 + round((H - kh)/2);
    y  = clamp(y, 1, nrows - kh + 1);
    kernels = struct('x',{},'y',{},'w',{},'h',{});
    for x = xs
        k.x = clamp(round(x), 1, ncols - kw + 1);
        k.y = y; k.w = kw; k.h = kh;
        kernels(end+1) = k; %#ok<AGROW>
    end
end

function c = ncc_scalar(A,B)
    A = A - mean(A(:)); B = B - mean(B(:));
    denom = sqrt(sum(A(:).^2) * sum(B(:).^2));
    if denom==0, c=0; else, c = sum(A(:).*B(:))/denom; end
end

function d_sub = subpixel_quadratic(y, idx)
    y1 = y(idx-1); y2 = y(idx); y3 = y(idx+1);
    denom = (y1 - 2*y2 + y3);
    if denom==0, delta=0; else, delta = 0.5*(y1 - y3)/denom; end
    d_sub = delta;
end

function customWait(hROI)
    l = addlistener(hROI, 'ROIClicked', @clickCb);
    uiwait; delete(l);
    function clickCb(~, evt)
        if strcmp(evt.SelectionType, 'double'), uiresume; end
    end
end
```

8.2 Longitudinal wall displacement and velocity per Subject

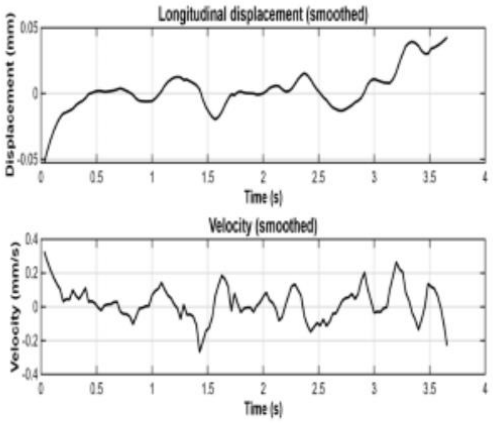

Subject 1

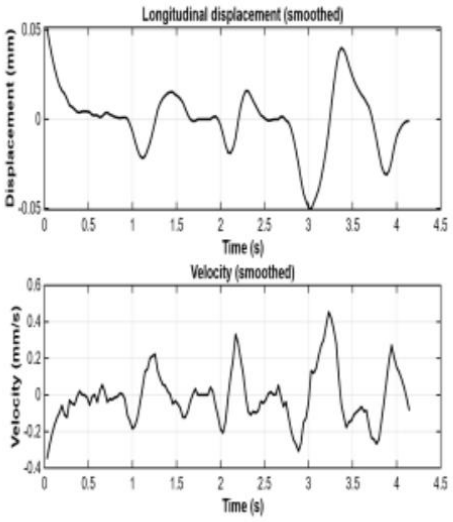

Subject 2 (left)

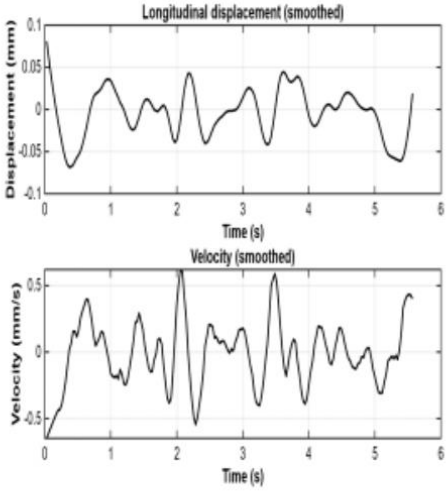

Subject 2 (right)

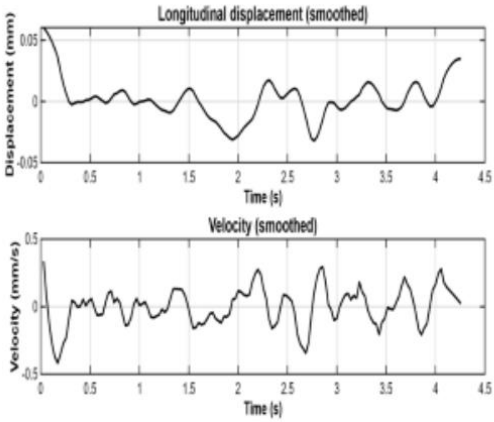

Subject 3

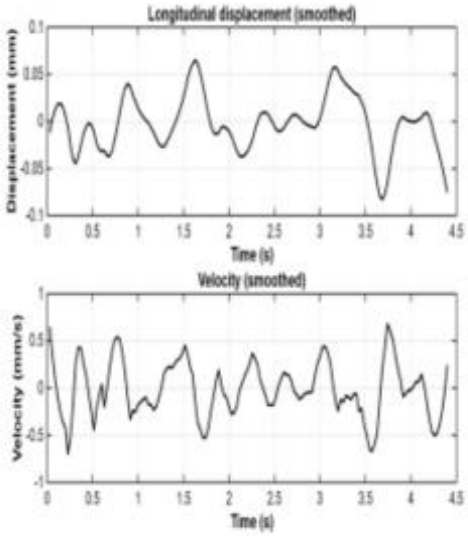

Subject 4

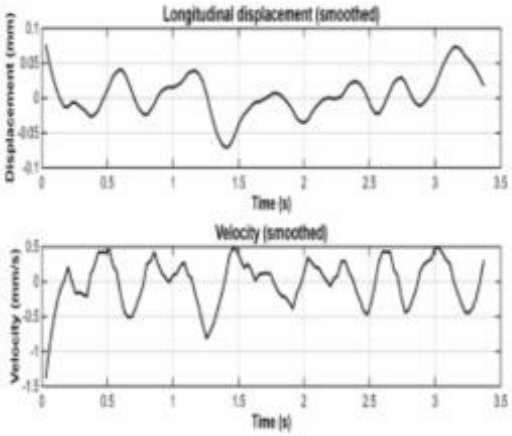

Subject 5

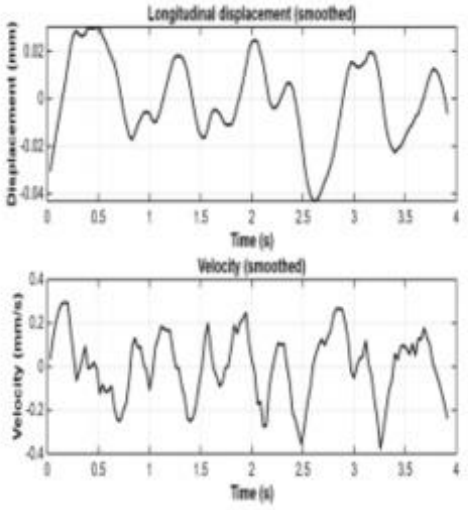

Subject 6 (left)

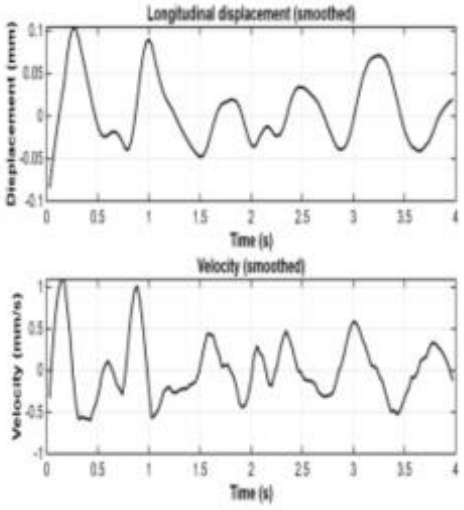

Subject 6 (right)

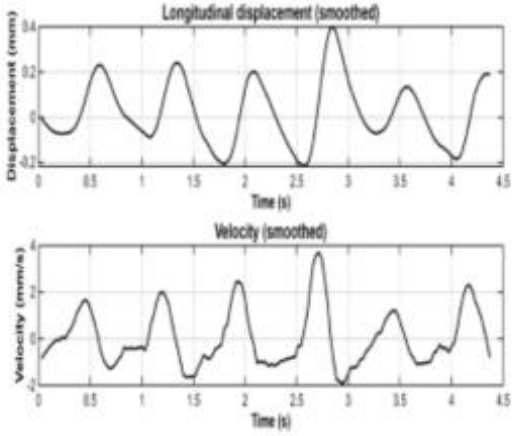

Subject 7

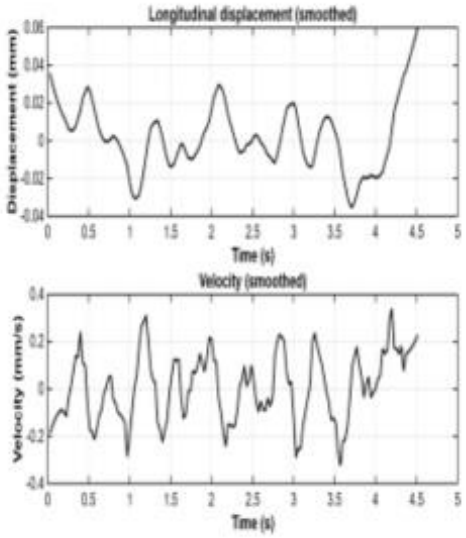

Subject 8 (left)

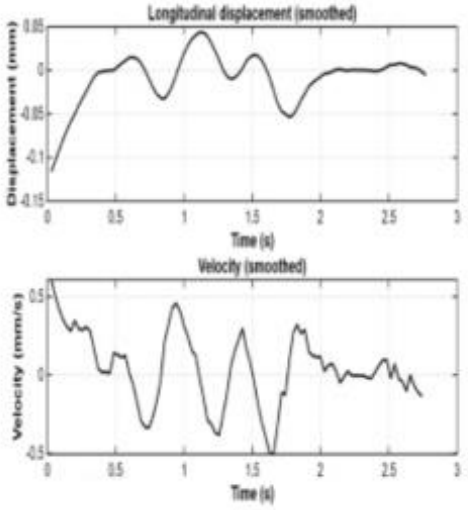

Subject 8 (right)

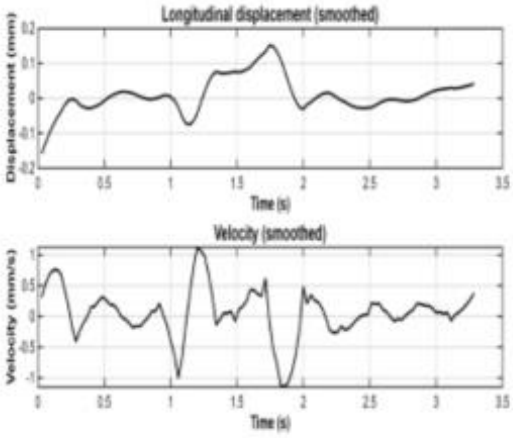

Subject 9 (left)

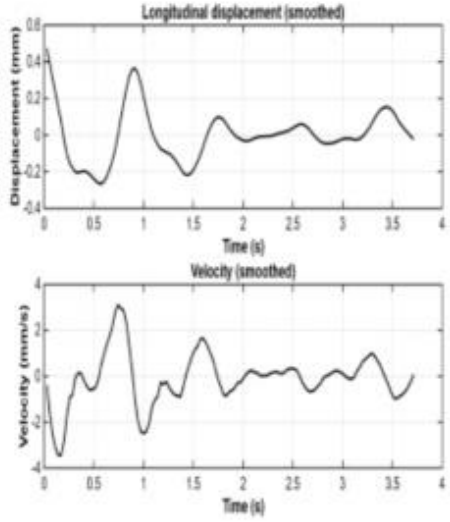

Subject 9 (right)

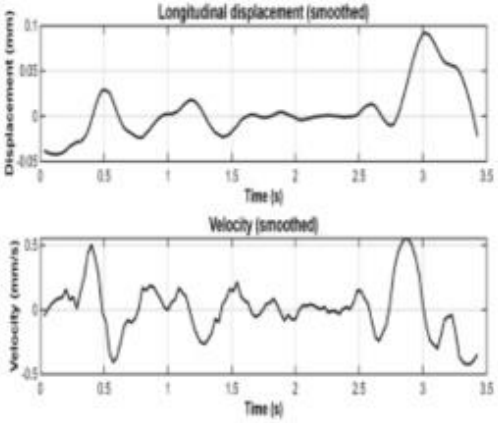

Subject 10

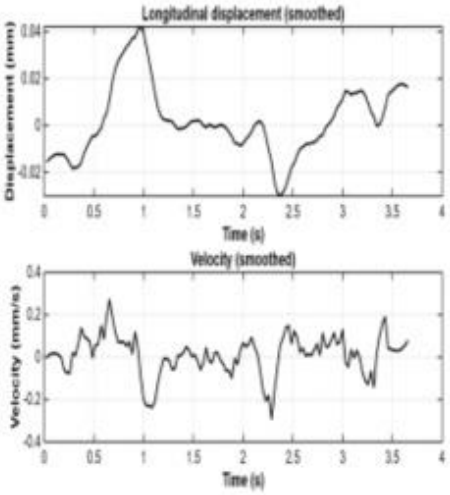

Subject 11 (left)

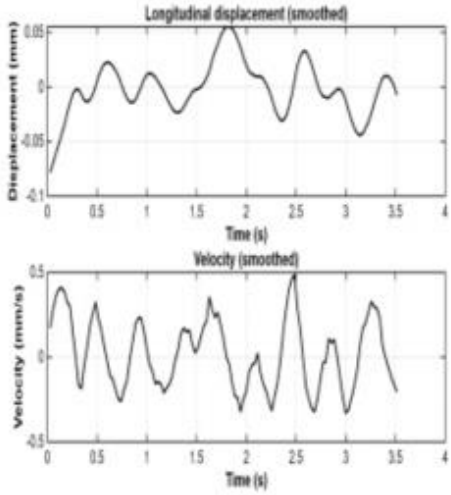

Subject 11 (right)

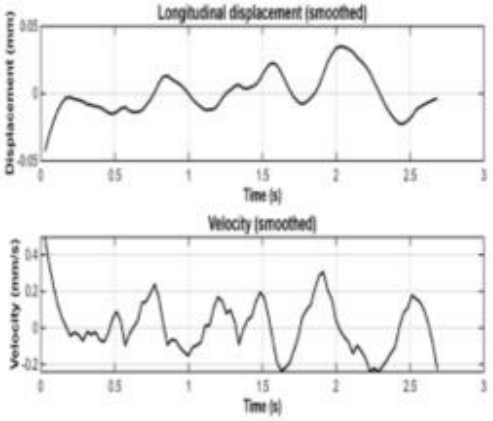

Subject 12

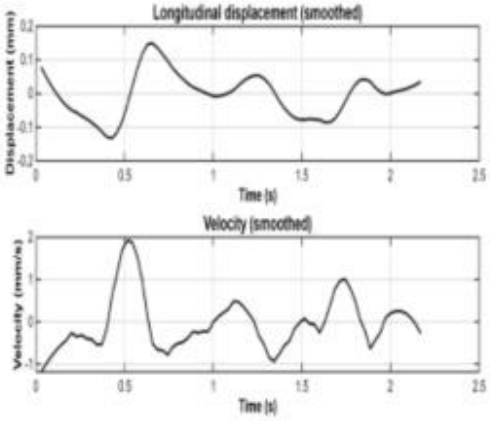

Subject 13

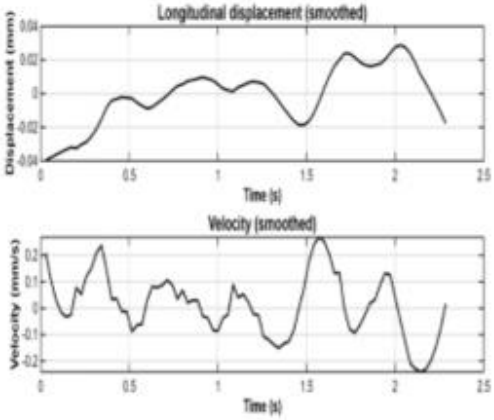

Subject 14

8.3 Diameter waveform variation per Subject

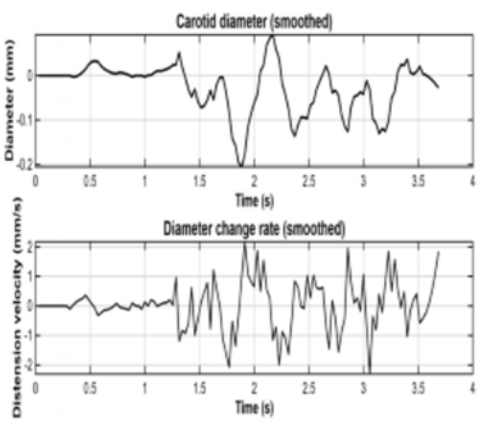

Subject 1

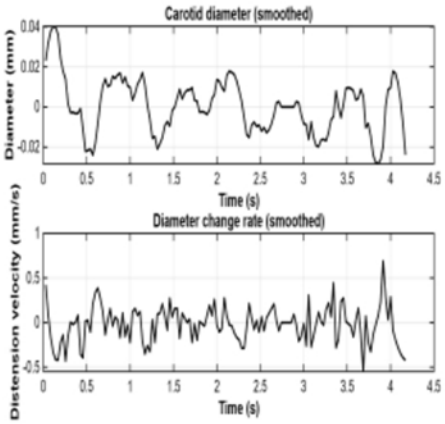

Subject 2 (left)

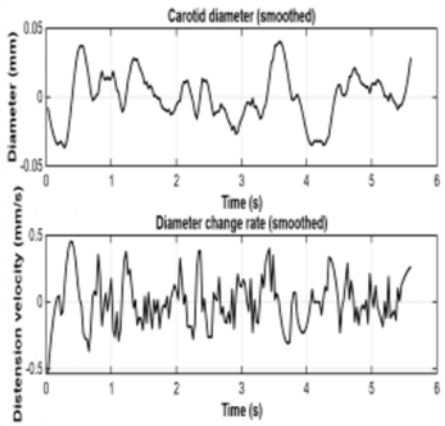

Subject 2 (right)

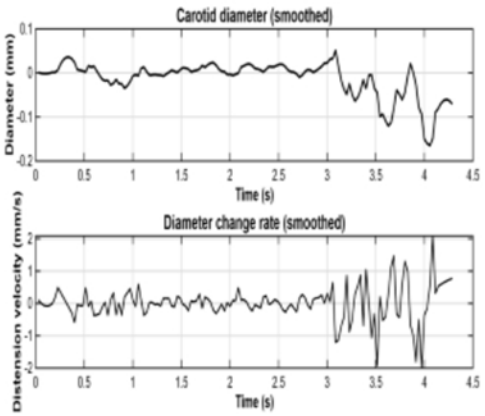

Subject 3

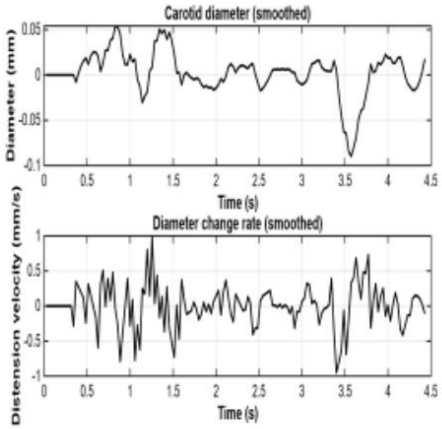

Subject 4

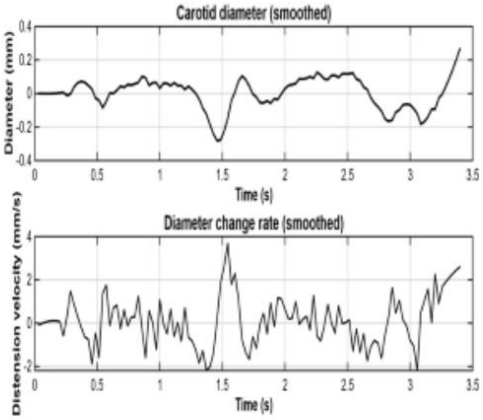

Subject 5

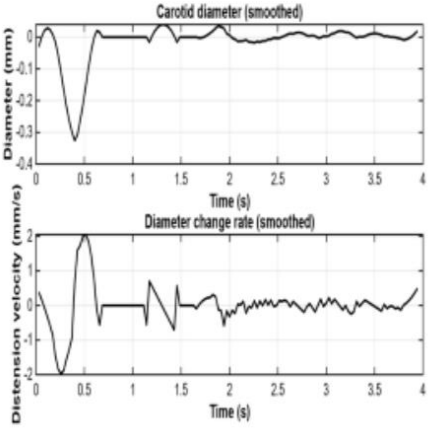

Subject 6 (left)

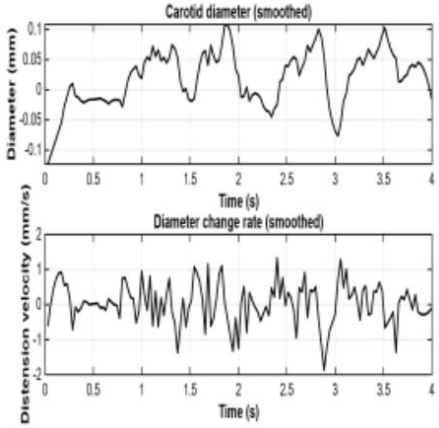

Subject 6 (right)

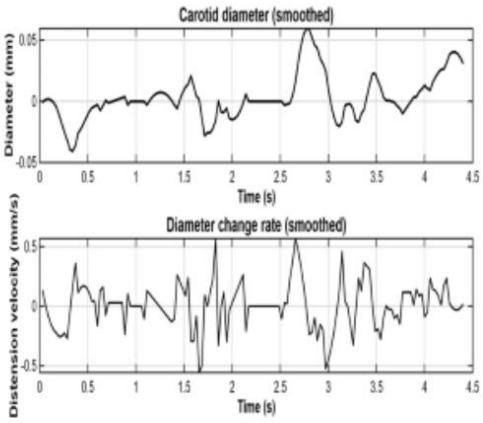

Subject 7

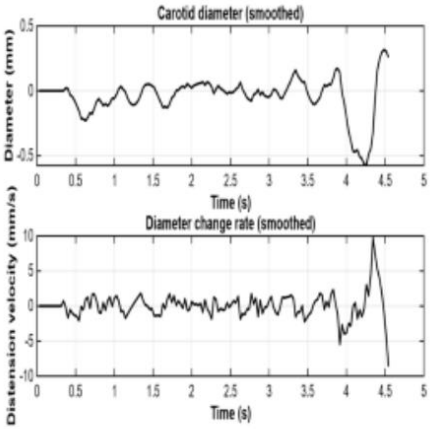

Subject 8 (left)

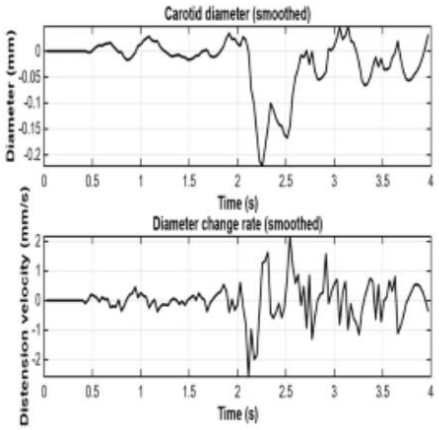

Subject 8 (right)

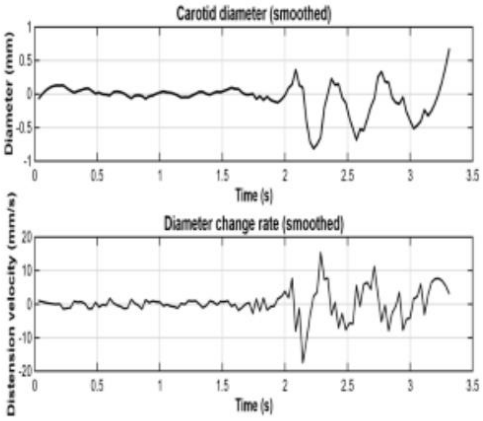

Subject 9 (left)

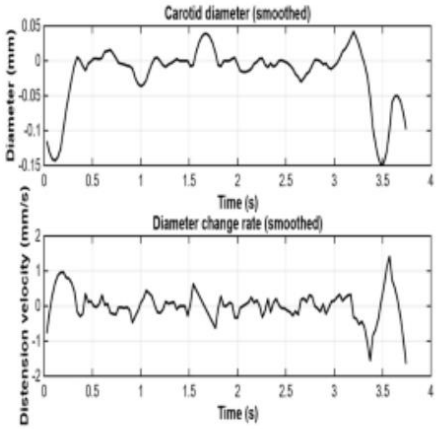

Subject 9 (right)

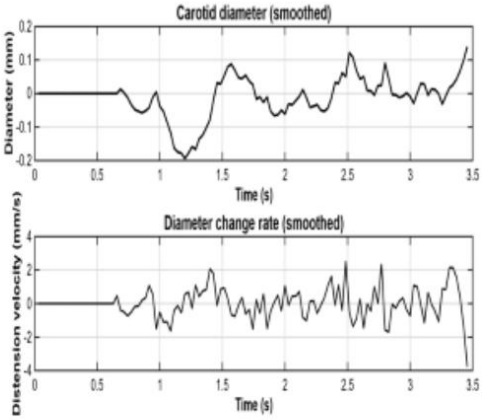

Subject 10

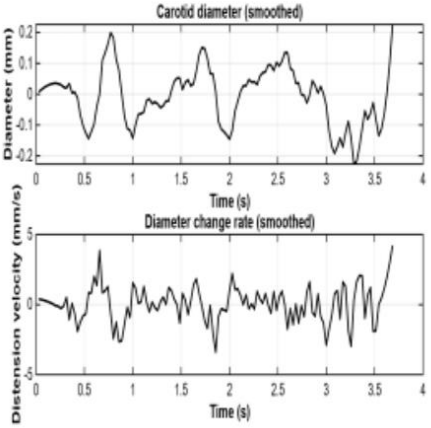

Subject 11 (left)

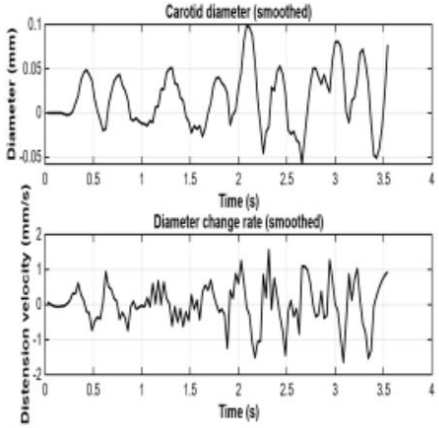

Subject 11 (right)

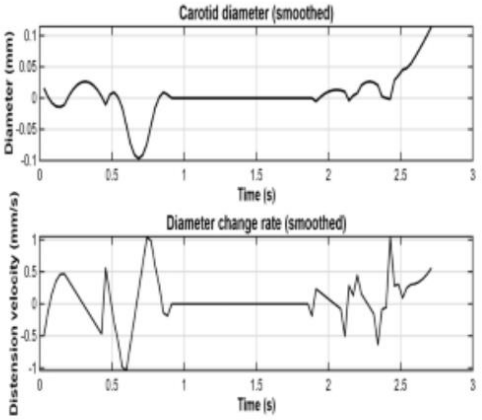

Subject 12

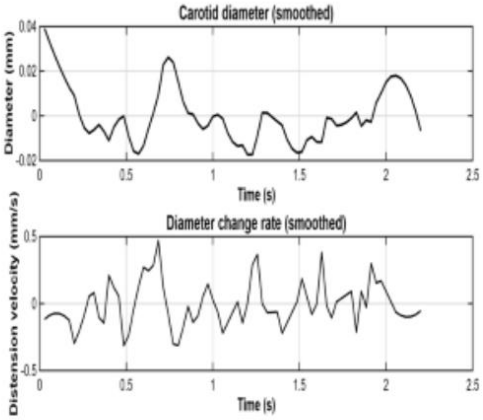

Subject 13

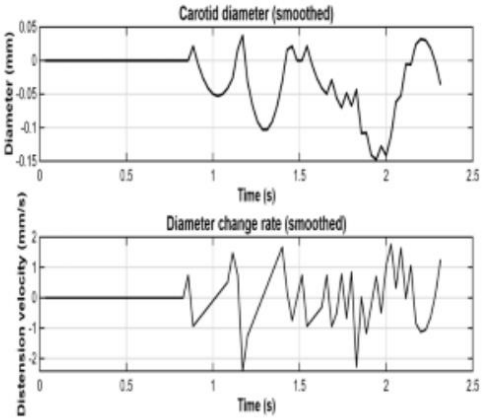

Subject 14